



HAL
open science

Human erythroid differentiation requires VDAC1-mediated mitochondrial clearance

Martina Moras, Claude Hattab, Pedro Gonzalez-Menendez, Claudio Fader,
Michael Dussiot, Jerome Larghero, Caroline Le van Kim, Sandrina Kinet,
Naomi Taylor, Sophie Lefevre, et al.

► **To cite this version:**

Martina Moras, Claude Hattab, Pedro Gonzalez-Menendez, Claudio Fader, Michael Dussiot, et al..
Human erythroid differentiation requires VDAC1-mediated mitochondrial clearance. *Haematologica*,
2020, 10.3324/haematol.2020.257121 . halshs-03429293

HAL Id: halshs-03429293

<https://shs.hal.science/halshs-03429293>

Submitted on 24 Nov 2021

HAL is a multi-disciplinary open access archive for the deposit and dissemination of scientific research documents, whether they are published or not. The documents may come from teaching and research institutions in France or abroad, or from public or private research centers.

L'archive ouverte pluridisciplinaire **HAL**, est destinée au dépôt et à la diffusion de documents scientifiques de niveau recherche, publiés ou non, émanant des établissements d'enseignement et de recherche français ou étrangers, des laboratoires publics ou privés.

Human erythroid differentiation requires VDAC1-mediated mitochondrial clearance

by Martina Moras, Claude Hattab, Pedro Gonzalez-Menendez, Claudio M. Fader, Michael Dussiot, Jerome Larghero, Caroline Le Van Kim, Sandrina Kinet, Naomi Taylor, Sophie D. Lefevre, and Mariano A. Ostuni

Haematologica 2020 [Epub ahead of print]

Citation: Martina Moras, Claude Hattab, Pedro Gonzalez-Menendez, Claudio M. Fader, Michael Dussiot, Jerome Larghero, Caroline Le Van Kim, Sandrina Kinet, Naomi Taylor, Sophie D. Lefevre, and Mariano A. Ostuni. Human erythroid differentiation requires VDAC1-mediated mitochondrial clearance.

Haematologica. 2020; 105:xxx

doi:10.3324/haematol.2020.257121

Publisher's Disclaimer.

E-publishing ahead of print is increasingly important for the rapid dissemination of science. Haematologica is, therefore, E-publishing PDF files of an early version of manuscripts that have completed a regular peer review and have been accepted for publication. E-publishing of this PDF file has been approved by the authors. After having E-published Ahead of Print, manuscripts will then undergo technical and English editing, typesetting, proof correction and be presented for the authors' final approval; the final version of the manuscript will then appear in print on a regular issue of the journal. All legal disclaimers that apply to the journal also pertain to this production process.

Human erythroid differentiation requires VDAC1-mediated mitochondrial clearance

Martina Moras^{1,2,3}, Claude Hattab^{1,2,3}, Pedro Gonzalez-Menendez^{3,4}, Claudio M. Fader^{5,6}, Michael Dussiot^{3,7}, Jerome Larghero⁸, Caroline Le Van Kim^{1,2,3}, Sandrina Kinet^{3,4}, Naomi Taylor^{3,4,9}, Sophie D. Lefevre^{1,2,3#}, Mariano A. Ostuni^{1,2,3#}

- 1) Université de Paris, UMR_S1134, BIGR, Inserm, F-75015 Paris, France
 - 2) Institut National de Transfusion Sanguine, F-75015 Paris, France
 - 3) Laboratoire d'Excellence GR-Ex, F-75015, Paris, France
 - 4) Institut de Génétique Moléculaire de Montpellier, Univ Montpellier, CNRS, Montpellier, France
 - 5) Laboratorio de Biología Celular y Molecular, Instituto de Histología y Embriología (IHEM), Universidad Nacional de Cuyo, CONICET, Mendoza, Argentina.
 - 6) Facultad de Odontología, Universidad Nacional de Cuyo, Mendoza, Argentina.
 - 7) Université de Paris, UMR_S1163, Laboratory of Cellular and Molecular Mechanisms of Hematological Disorders and Therapeutical Implication, Inserm, F-75014 Paris, France.
 - 8) AP-HP, Hôpital Saint-Louis, Unité de Thérapie cellulaire, Paris, France.
 - 9) Pediatric Oncology Branch, Center for Cancer Research (CCR), National Cancer Institute (NCI), National Institutes of Health (NIH), Bethesda, Maryland, USA
- # These authors have equally contributed to this work

Running Head: **VDAC-driven mitophagy in human erythropoiesis**

Corresponding authors

Mariano A. OSTUNI and Sophie D. LEFEVRE

UMR_S1134 Biologie Intégrée du Globule Rouge

6, rue Alexandre Cabanel

75739 Paris cedex 15, FRANCE

Email address: mariano.ostuni@inserm.fr; sophie.lefevre@inserm.fr

Phone: +33 1 44 49 31 35

Fax: +33 1 43 06 50 19

Word Count:

Abstract: 142

Main text: 3465

Number of figures: 6 main figures and 1 pdf file including 6 Supplementary Figures

Acknowledgments

The authors would like to thank Mrs Corentine Chrysostome et Mr Abdellah Nait for their secretarial and technical assistance, respectively. We acknowledge the Cell Sorting facility of the Institut Imagine; the ImagoSeine core facility of the Institut Jacques Monod, member of IBiSA and France-BioImaging (ANR-10-INBS-04) infrastructure; the Laboratory of Excellence GR-Ex (Grant ANR-11-LABX-0051) and the Guests Researcher program from Paris Diderot University. Martina Moras is funded by the European Union's Horizon 2020

research and innovation program under the Marie Skłodowska-Curie grant agreement No. 665850, the Club du Globule Rouge et du Fer (CGRF) and Société Française d'Hématologie (SFH). Pedro Gonzalez-Menendez is funded by the CLARIN-COFUND program from the Principado de Asturias and the European Union.

Abstract

Erythroblast maturation in mammals is dependent on organelle clearance throughout terminal erythropoiesis. We studied the role of the outer mitochondrial membrane protein VDAC1 (Voltage-Dependent Anion Channel-1) in human terminal erythropoiesis. We show that shRNA-mediated downregulation of VDAC1 accelerates erythroblast maturation. Thereafter, erythroblasts are blocked at orthochromatic stage, exhibiting a significant decreased level of enucleation, concomitant with an increased cell death. We demonstrate that mitochondria clearance starts at the transition from basophilic to polychromatic erythroblast, and that VDAC1 downregulation induces the mitochondrial retention. In damaged mitochondria from non-erythroid cells, VDAC1 was identified as a target for Parkin-mediated ubiquitination to recruit the phagophore. Here, we showed that VDAC1 is involved in phagophore's membrane recruitment regulating selective mitophagy of still functional mitochondria from human erythroblasts.

These findings demonstrate for the first time a crucial role for VDAC1 in human erythroblast terminal differentiation, regulating mitochondria clearance.

Introduction

Mature erythrocytes result from a finely regulated process called erythropoiesis, producing two million erythrocytes every second in healthy human adults (1). In mammals, during the late stages of terminal erythroid differentiation, erythroblasts expel their nuclei and lose their organelles including the Golgi apparatus, endoplasmic reticulum (ER), ribosomes and mitochondria (2). Organelles can be eliminated by the general process of macro-autophagy. This process is initiated by the formation of a double membrane structure called phagophore, engulfing cytoplasmic material to form the autophagosome which fuses with a lysosome for degradation (3). Alternatively, mitochondria can be eliminated by a selective autophagic process called mitophagy, in which outer mitochondrial membrane (OMM) proteins act as signals to recruit the phagophore membrane (4). In erythroid progenitors, much work has shown that autophagy is essential for the organelle removal that occurs during reticulocyte maturation (5, 6). Notably though, the majority of these studies were performed in human progenitors that had already reached the reticulocyte stage of differentiation or in genetic mouse models that were deleted for different proteins involved in phagophore formation (i.e. Ulk1, Atg4, Atg7). In these latter models, the importance of autophagy in murine erythroid differentiation was demonstrated by the finding that the delayed clearance of mitochondria and ribosomes is associated with anemia (7-11).

Mitophagy results from the binding of adaptors to LC3 (microtubule-associated protein 1 light chain 3B, also known as ATG8) within the growing autophagosome. Once associated with phosphatidyl ethanolamine (PE), LC3-II (PE-conjugated LC3) enables the elongation and maturation of the phagophore that is recruited to ubiquitin-covered mitochondria through interaction with the LIR (LC3-interacting region) motif of mitophagy adaptors. An autophagosome is then built around mitochondria that are finally degraded following autophagosome-lysosome fusion. Mitophagy can also occur in an ubiquitin-independent manner following accumulation of OMM proteins such as NIX/BNIP3L (12), bringing together autophagosomal membranes and mitochondria via their LIR motif (4). In this regard, it is interesting to note that the absence of NIX results in mitochondrial retention and anemia in mice (12-14).

The PINK1/Parkin pathway is one of the best-characterized pathways of mitophagy. In healthy functional mitochondria, PINK1 (PTEN-induced putative kinase 1) is addressed to the OMM. Once translocated to the inner membrane, this protein is cleaved and targeted for degradation by the proteasome. However, on defective mitochondria, there is an accumulation

of PINK1 which results in the translocation of Parkin, an E3 ubiquitin ligase, and the subsequent clearance of damaged mitochondria by mitophagy (15-17).

At the surface of damaged mitochondria, Parkin interacts with OMM proteins among which voltage-dependent anion channels (VDACs). Furthermore, in the absence of all three VDACs, mitophagy has been shown to be impaired, at least in certain cell types (18-20).

VDAC1 is a ubiquitous OMM protein involved in different pathways including apoptosis (21, 22), mitochondrial cristae scaffold (23), and nucleotides transport (24, 25), its role in erythropoiesis is not known, but transcriptomic and proteomic data could suggest a role at the terminal differentiation (26, 27). Using a shRNA approach, we find that downregulation of VDAC1 results in a blockage in erythroid progenitor differentiation at the orthochromatic erythroblast stage, exhibiting a significantly decreased level of enucleation and cell death.

Furthermore, we show that the clearance of mitochondria from terminal erythroblasts is dependent on VDAC1, starting at the polychromatic erythroblast stage of differentiation. VDAC1 plays a crucial role to initiate the recruitment of phagophore's membrane, necessary to achieve an efficient maturation of human red blood cells.

Methods

CD34⁺ cells isolation and ex vivo erythroid differentiation

CD34⁺ cells were isolated from cord blood and cultured following a human *ex vivo* differentiation protocol as previously described (28) (**Supplemental data**). The experimental protocol was approved by ethical committees from Inspire H2020 program (agreement 655850) and from INTS (2019-1), additional information is included as supplemental data.

Transduction of CD34⁺ progenitors

Cells undergoing erythroid differentiation were transduced at day 4 of erythroid differentiation with lentiviral vectors (MISSION® pLKO.1) containing a short hairpin RNA scramble (shSCR) or a short hairpin RNA targeting VDAC1 (shVDAC1) (TRCN0000297481) upstream of the EGFP transgene, at a MOI of 10 (**Figure S1A**). Transduction efficiency was evaluated by the percentage of EGFP⁺ cells after 72 h and EGFP⁺ cells were sorted using the cell sorter SONY SH800.

Flow cytometry-based analysis of erythroid differentiation

Cells were analyzed for surface markers expression, mitochondrial content and the presence of a nucleus, starting at day 7. Briefly, 10^5 cells were stained with 250 nM MitoFluor and Hoechst 34580 in media for 30 min at 37 °C. Cells were washed and subsequently stained with fluorochrome-conjugated antibodies against glycophorin A (GPA), Band3 and α 4-integrin in PBS 2% BSA, for 30 min at 4 °C. Cells were washed once with PBS and 7-AAD was added prior to acquisition to exclude dead cells. Cells were analyzed using a BD FACSCanto™ (BD Biosciences), data were acquired with Diva software and analyzed using FCS express 6 Flow Research Edition software.

Enucleation assay by imaging flow cytometry

Orthochromatic erythroblasts were sorted at day 12 as described (28). Cells were maintained in culture for one day in phase III medium before staining with 1 μ g/mL Hoechst 34580 and anti-GPA Ab. Nucleus polarization was analyzed by Amnis® Imaging Flow Cytometer. Approximately 10,000 events were collected and the “Delta centroid GPA-Hoechst” was calculated as the distance of the center of the GPA-labeled erythroblast from the center of the Hoechst-labeled nucleus. A threshold of 2 for the Delta Centroid (DC) was fixed in order to discriminate between polarized and non-polarized nucleus. Analysis was performed using the IDEAS 6.2 software (29).

Other standard methods.

Quantitative real time qPCR, antibodies and dyes, MGG-based identification of erythroblasts stage, apoptosis assay, ROS detection, mitochondrial respiration analysis, immunoblotting, immunolabelling for confocal microscopy, ATP measurement, electron microscopy, K562 cell culture, image stream colocalization and statistical analysis are fully described in supplementary material.

Results

shRNA-mediated knockdown of VDAC1 results in an accelerated erythropoiesis until the orthochromatic erythroblast stage of differentiation

In order to assess the specific effects of VDAC1 during erythroid differentiation, we pursued a shRNA-mediated knockdown approach. CD34⁺ cells were transduced at day 4 of differentiation with a sh-Scramble (shSCR) or a shVDAC1 lentiviral vector, both harboring the EGFP transgene (**Figure S1A**), and EGFP⁺ cells were sorted at day 7 (**Figure 1A**).

Knockdown efficiency was assessed at day 10 and a significant downregulation of VDAC1 expression, both at the mRNA ($53.6\% \pm 7.6$) and protein level ($78.5\% \pm 5.9$) was observed as compared to shSCR-transduced cells (**Figure S1B-C**). Of note, no significant difference was observed in the mRNA expression of two other VDACs, VDAC2 and VDAC3, confirming the specificity of the shRNA construct (**Figure S1D**).

The effect of VDAC1 downregulation on erythroblast maturation was assessed by quantifying the percentages of erythroblasts at different stages of differentiation, as monitored by MGG coloration. VDAC1 downregulation did not alter erythroid differentiation before 3 days post-transduction (D7) (**Figure 1B**). However, by day 10 of differentiation, shVDAC1-transduced cells exhibited an accelerated terminal differentiation as compared to control cells, shown by a significantly higher percentage of orthochromatic erythroblasts as compared to earlier basophilic and polychromatic erythroblasts (**Figure 1C**). These data were confirmed by evaluating $\alpha 4$ -integrin/Band3 profile by flow cytometry allowing the terminal stage of differentiation to be distinguished as previously described (28) (**Figure 1D**). Consistent with the data above, shVDAC1-transduced progenitors showed no difference in Band3 expression (**Figure 1E**) but a significantly decreased levels of $\alpha 4$ -integrin, a marker which is lost during terminal differentiation, as compared to shSCR-transduced cells (**Figure 1F**). Furthermore, we observed a decreased proliferation rate in shVDAC1-transduced cells starting at day 10 (**Figure 1G**). Altogether, these data point to the importance of VDAC1 in regulating terminal erythroid differentiation.

VDAC1 downregulation impairs erythroblast enucleation.

The main morphological feature of terminal mammalian erythroid differentiation is the enucleation, leading to the production of a reticulocyte and a pyrenocyte from an orthochromatic erythroblast. Despite the accelerated differentiation observed in shVDAC1-transduced cells, orthochromatic erythroblast percentage was increased whereas reticulocyte level was significantly decreased from day 14 until day 17 as evaluated by MGG coloration (**Figure 2A-B**) as well as Hoechst staining (**Figure 2C**).

Enucleation starts with the polarization of the nucleus towards the plasma membrane, allowing the separation of the nucleus from the yet-to-be formed reticulocyte by a mechanism similar to cytokinesis (30). To assess whether the decrease in enucleation in shVDAC1-transduced cells was due to an impairment in the polarization of the nucleus, we sorted orthochromatic erythroblasts at day 12 of differentiation and analyzed these cells by imaging flow cytometry 24 h later. We measured the distance between the center of the cell and the

center of the nucleus (delta centroid XY from the IDEAS software). No significant differences in delta centroid XY were observed between shVDAC1- and shSCR-transduced cells, suggesting that VDAC1 downregulation does not block the polarization of the nucleus (**Figure S2**).

To assess whether the block in enucleation affects cell viability, we evaluated the level of apoptosis as a function of Annexin V staining of exposed phosphatidylserine. While Annexin V staining was not altered in shVDAC1-transduced cells as compared to shSCR-transduced cells at days 7 and 10 of differentiation, levels were significantly higher at days 14 and 17, strongly suggesting that an attenuated enucleation was associated with apoptosis (**Figure 2D**).

Mitochondrial biomass remains elevated in shVDAC1-transduced erythroblasts.

In mammals, mature red blood cells are devoid of mitochondria. However, mitochondria can still be found at the reticulocyte stage in many mammalian species such as rabbits, dogs, rats, mice and humans (5, 31-33). As expected, we detected a progressive decrease in mitochondrial biomass during erythroblast maturation, with a first major decrease in the transition between basophilic and polychromatic stages and a second between polychromatic and orthochromatic stages (**Figure 3A**). At day 10 of differentiation the mitochondrial marker TOM40 was detected at significantly higher levels in shVDAC1-transduced cells by Western blot analysis (2.6 ± 0.6 -fold, $n = 5$; **Figure 3B**). As VDAC1 downregulation alters the kinetic of differentiation, difference on protein expression at day 10 could result from a different proportion of erythroblastic stages. For this reason, mitochondrial biomass was assessed by flow cytometry in the different stages based on α -4integrin/Band3 profile as previously described. Mitochondrial biomass was significantly higher in shVDAC1-polychromatic and orthochromatic erythroblasts as compared to shSCR-transduced erythroblasts (**Figure 3C**). Importantly, these differences were associated with late stages of differentiation as there was no change in mitochondrial biomass in earlier basophilic erythroblasts. Although shSCR transduced cells progressively eliminate mitochondria at each differentiation stage, our data point to a defect in mitochondrial clearance during the transition between basophilic and polychromatic erythroblasts in conditions of VDAC1 downregulation.

VDAC1 regulates mitochondrial morphology and oxidative phosphorylation in terminal erythroblasts

To evaluate mitochondrial function in shVDAC1-transduced erythroblasts, we first evaluated the structural morphology of mitochondria by transmission electron microscopy at

day 10 of differentiation (**Figures 4A and S3**). In contrast with the normal ultrastructural morphology detected in shSCR-transduced cells, shVDAC1-transduced cells exhibited swollen mitochondrial cristae (**Figure 4A-B**) with a significantly increased percentage of rounded as compared to elongated mitochondria ($p < 0.0001$, **Figures 4A-C**). These data are in agreement with a published role of VDAC1 OMM-IMM contacts sites in cristae structuration (23). Interestingly, we also observed a reduced number of ER-mitochondria contact sites in shVDAC1-transduced cells (**Figure 4D**). As these mitochondrial associated membranes have been shown to recruit signaling molecules such as mTOR, GSK3 and hexokinase I, thereby increasing oxidative phosphorylation (34), it was of interest to evaluate mitochondrial function in erythroblasts with downregulated VDAC1. Notably, shVDAC1-transduced erythroblasts exhibited a significantly decreased oxygen consumption rate, evaluated as a function of mitochondrial biomass (**Figure 4E**). This measure, quantifying oxidative phosphorylation (OXPHOS), was lower in shVDAC1-transduced erythroblasts for both basal levels and maximal respiration (**Figure 4F**). In accord with the lower OXPHOS, intracellular ATP levels were significantly lower in shVDAC1-transduced cells than control cells (**Figure 4G**). We also measured mitochondria membrane potential and ROS accumulation at day 10 and showed no difference in cells transduced with shVDAC1 compared to the shSCR (**Figure S4**), suggesting an adaptation of the cell to compensate for mitochondria changes of metabolism upon VDAC1 downregulation. Thus, decreased expression of VDAC1 attenuates mitochondrial function, resulting in a diminished energetic state of the differentiating erythroblast.

Delayed mitochondrial clearance in late-stage erythroblasts with downregulated VDAC1 is due to a defective recruitment of autophagosomal membranes.

Given that VDAC1 has been shown to regulate mitophagy in non-erythroid cell lines (18-20), we hypothesized that VDAC1 downregulation could impair mitophagy in human erythroblasts as well. While the autophagy-mediated lipidation of LC3-I to LC3-II in the autophagosome membrane was not altered upon VDAC1 downregulation (**Figure 5B**), there was a significant accumulation of p62, an adaptor protein that allows bridging between the ubiquitinated cargos and the phagophore membrane (35) (**Figure 5A-5C**). Furthermore, p62 expression was detected by flow cytometry in different stages on fixed cells stained with $\alpha 4$ -integrin and Band3 antibodies. As well as for mitochondrial content, a significant increase in p62 was observed at polychromatic and orthochromatic stages in shVDAC1-transduced cells (**Figure 5D**).

After engulfment of the mitochondria, the autophagosome usually fuses with a lysosome, leading to the degradation of the mitochondria along with the adaptor proteins (**Figure 5A**). To decipher whether p62 accumulation was due to a stabilization at MOM on ubiquitinated proteins or to a defect in mitophagy completion by lysosomal degradation, we studied the autophagosomal membrane recruitment to mitochondria by immunofluorescence. We observed a significant decreased colocalization between autophagosomal LC3-II and the mitochondrial marker TOM22 in shVDAC1-transduced cells ($p < 0.01$; **Figure 5E**), suggesting a defect in the phagophore membrane recruitment and consequently a defect in mitophagy completion.

To assess the specificity of our results, we constructed shSCR-K562 and shVDAC1-K562 stable cell lines and transfected shSCR-K562 cells with a siRNA against VDAC1 (siVDAC1-K562). We confirmed by Western blot VDAC1 downregulation (**Figure S5A**), and showed, as for differentiating erythroblasts, no difference in LC3 activation (**Figure S5B**) and an increase in p62 protein level (**Figure S5C**). We also observed a decrease of LC3/TOM22 colocalization in shVDAC1-K562 and siVDAC1-K562, which indicates the recruitment of the phagophore membrane to the mitochondria was impaired upon VDAC1 downregulation (**Figure S5D**). These data confirmed that VDAC1 downregulation in K562 erythroid cells recapitulates the phenotype observed on VDAC1-downregulated erythroblasts.

PINK1 protein level is reduced upon VDAC1 downregulation

The phagophore recruitment is dependent of some specific MOM proteins stabilization and direct or indirect interaction with lipidated LC3 (**Figure 5A**). We first evaluated NIX levels, previously identified in mouse reticulocytes as being critical for the recruitment of autophagosomal membranes and appropriate mitophagy (36). Notably, we did not detect a significant decrease in either NIX dimers or NIX transcripts in human erythroblasts with decreased VDAC1 expression (**Figure S6**). We then studied the second main mitophagy induction pathway and observed by Western blot a significant decrease of full-length PINK1 protein level in shVDAC1-transduced bulk erythroblasts at D10 (**Figure 6A**). PINK1 expression was then evaluated by flow cytometry on basophilic, polychromatic and orthochromatic erythroblasts based on $\alpha 4$ -integrin and Band3 expression pattern. We confirmed a significant decrease of PINK1 level starting from the polychromatic stage (**Figure 6B**), in line with the differences of mitochondrial mass and p62 expression.

We next confirmed on K562 cell lines the reduction of PINK1 protein level upon VDAC1 downregulation (**Figure 6C**). Furthermore, we observed a reduction of the mitochondrial

localization of PINK1, as shown by the reduction of PINK1/TOM22 colocalization in shVDAC1-K562 cells (**Figure 6D**). Finally, we observed a decrease of the phagophore recruitment to the mitochondria when downregulating PINK1 on shSCR-K562, as observed with the significant reduction LC3/TOM22 colocalization (**Figure 6E**). In contrast, LC3/TOM22 colocalization is not worsened upon PINK1 down-regulation on shVDAC1-K562 cells (**Figure 6E**).

Discussion

Mitochondrial clearance is a crucial process for the production of mature red blood cells and several studies have shown that mitophagy occurs at the reticulocyte stage, allowing the complete clearance of mitochondria and final murine erythrocyte maturation (13, 14). Mitophagy is a mitochondrial-specific form of general macroautophagy, which can be mediated by different well characterized pathways involving proteins signaling as the PINK1/Parkin pathway, NIX and BNIP3. While autophagy related genes (ATG) have been shown to be critical for mitochondrial clearance during erythropoiesis (6-11), and the NIX-driven pathway has been identified as playing a role in murine erythropoiesis (12-14), the importance of these mitophagy pathways in human erythroid terminal differentiation is not known.

Here we focused on the role of VDAC1, an OMM protein, known to be involved in mitophagy in non-erythroid cells.

We find that VDAC1 downregulation accelerates human erythroblast differentiation until the orthochromatic erythroblast stage, but then blocks enucleation and cumulates mitochondria with altered ultrastructure and decreased function, resulting in apoptosis.

In agreement with previous data on the role of VDAC1 in the structuration of mitochondria (23), we observed altered mitochondria ultrastructure and a decrease in ER-mitochondria contact sites in shVDAC1-transduced erythroblasts by electron microscopy. Notably, complexes between VDAC and hexokinase-1 at ER-mitochondrial contact sites have been shown to regulate mitochondrial metabolism (34). In our study, mitochondria in VDAC1-downregulated erythroblasts showed a decrease in OCR and intracellular ATP content, a signature of reduced mitochondrial activity. Thus, perturbations in mitochondrial metabolism may influence the kinetics of erythroblast differentiation and their enucleation profiles.

We demonstrated that VDAC1 is required for progressive mitochondrial clearance during the terminal phase of differentiation. This is in line with a previous study showing a decrease in mitochondrial mass after the proerythroblastic stage (37). We found that this is regulated through the PINK1/Parkin pathway, with VDAC1 modulating PINK1 accumulation at the mitochondria outer membrane and the recruitment of the phagophore. Accordingly, the attenuation of mitochondrial clearance was associated with increased levels of p62, an adaptor protein that allows bridging between the ubiquitinated cargos and the phagophore membrane (35).

Our data therefore highlight the critical role of VDAC1 function in the recognition of mitochondria that are “to be degraded” during the process of red cell maturation. We recently demonstrated that TSPO1 downregulation also affects mitochondria clearance with no effect on the erythroblasts’ differentiation kinetic (38), raising the possibility that this phenotype is mediated through the VDAC1-TSPO1 OMM complex.

In addition, our findings suggest that the canonical PINK1/Parkin pathway may play an important role during human erythropoiesis, confirming in humans previous study on mice (39). Transcriptome analyses in human erythroblasts detected an upregulation, starting from the polychromatic stage, of key proteins of mitophagy belonging to different pathways, such as NIX and PINK1 (26). NIX upregulation was described by several works studying NIX-mediated mitophagy in murine reticulocytes (12-14), but no clear evidence was found to explain the upregulation of PINK1. Under condition of VDAC1 downregulation, NIX protein levels were not altered, suggesting that mitochondrial retention was not due to a defect in the NIX pathway but in the PINK1 pathway, as described below. It was previously reported that VDAC is required to promote Parkin recruitment to the mitochondria (18). Our data suggest that this could be due to a lack in PINK1 accumulation at the OMM.

Since VDAC1 is part of a multimeric complex with ATAD3A (23), we speculate that in the absence of VDAC1, ATAD3A is free to form alternative complexes (40). Recently, a new function of ATAD3A was described in hematopoietic progenitor cells, promoting the import of PINK1 (41). In this context PINK1 is rapidly degraded by the mitochondrial peptidases MPP and Parl to prevent its accumulation in the surface prevent mitophagy. However, when ATAD3A dissociates from the translocase of the inner membrane (TIM) complex, the import of PINK1 is blocked, causing its accumulation (42). It is noteworthy that also hexokinase 2 (HK2) and adenine nucleotides transporter (ANT) both proteins know to be involved in a multimeric mitochondrial membrane protein complex, have been recently shown to be essential for PINK1 accumulation at the OMM (43, 44), suggesting a role of this complex in

PINK1/parkin mitophagy. Further studies are necessary to assess this hypothesis and evaluate the crosstalk between VDAC1, ATAD3A, ANT and/or HK2 in the terminal phase of erythropoiesis.

In conclusion, our data are the first demonstration of a fundamental role of mitochondrial-selective autophagy at the erythroblast stage. Loss of VDAC1 causes an ineffective elimination of mitochondria in the transition between basophilic and orthochromatic erythroblasts, demonstrating the critical role of VDAC1 in late stage erythropoiesis.

We have taken account of recent report highlighting the possible unspecific and strain-dependent effects of shRNA knocking down on mouse erythroblasts enucleation (45). However, we have observed the same effects knocking down VDAC1 by two different approaches (shRNA and siRNA) and using different experimental models, strongly supporting our conclusions.

Over the last few years, several studies have demonstrated the association of mitophagy defects with various hematological syndromes, highlighting the importance of mitochondrial content and mitophagy during human erythropoiesis (46-53). Our work provides a better understanding of the mechanisms regulating mitochondrial autophagy in human erythroid progenitors, particularly during the terminal phase of erythropoiesis. Elucidating the different pathways involved in mitochondrial clearance and their kinetics, will promote the development of novel therapeutic approaches for treating hematological disorders that involves defective erythroid maturation.

Authorship Contributions

MM designed experiments, performed experiments, analyzed data and wrote the paper. CH, PGM, MD, SK and CF performed experiments. JL evaluated protocols and supervised blood samples purchasing. CLVK critically evaluated experiments and obtained funding, SK and NT critically evaluated experiments, provided supervision, wrote the paper and obtained funding. SDL and MAO conceived the project, obtained funding, designed and critically evaluated experiments, provided supervision and wrote the paper; they equally contributed to this paper. All authors read and commented on the paper and approved the final version.

Disclosures of conflict of Interest

The authors declare that they have no financial interest that might influence the results or interpretation of their manuscript.

References

1. Palis J. Primitive and definitive erythropoiesis in mammals. *Front Physiol.* 2014;5:3.
2. Moras M, Lefevre SD, Ostuni MA. From Erythroblasts to Mature Red Blood Cells: Organelle Clearance in Mammals. *Front Physiol.* 2017;8:1076.
3. Klionsky DJ. The molecular machinery of autophagy: unanswered questions. *J Cell Sci.* 2005;118(Pt 1):7-18.
4. Liu L, Sakakibara K, Chen Q, Okamoto K. Receptor-mediated mitophagy in yeast and mammalian systems. *Cell Res.* 2014;24(7):787-795.
5. Kent G, Minick OT, Volini FI, Orfei E. Autophagic vacuoles in human red cells. *Am J Pathol.* 1966;48(5):831-857.
6. Zhang J, Wu K, Xiao X, et al. Autophagy as a regulatory component of erythropoiesis. *Int J Mol Sci.* 2015;16(2): 4083-4094.
7. Honda S, Arakawa S, Nishida Y, Yamaguchi H, Ishii E, Shimizu S. Ulk1-mediated Atg5-independent macroautophagy mediates elimination of mitochondria from embryonic reticulocytes. *Nat Commun.* 2014;5:4004.
8. Betin VM, Singleton BK, Parsons SF, Anstee DJ, Lane JD. Autophagy facilitates organelle clearance during differentiation of human erythroblasts: evidence for a role for ATG4 paralogs during autophagosome maturation. *Autophagy.* 2013;9(6):881-893.
9. Zhang J, Randall MS, Loyd MR, et al. Mitochondrial clearance is regulated by Atg7-dependent and -independent mechanisms during reticulocyte maturation. *Blood.* 2009;114(1):157-164.
10. Kundu M, Lindsten T, Yang CY, et al. Ulk1 plays a critical role in the autophagic clearance of mitochondria and ribosomes during reticulocyte maturation. *Blood.* 2008;112(4):1493-1502.
11. Mortensen M, Ferguson DJ, Edelmann M, et al. Loss of autophagy in erythroid cells leads to defective removal of mitochondria and severe anemia in vivo. *Proc Natl Acad Sci U S A.* 2010;107(2):832-837.
12. Novak I, Kirkin V, McEwan DG, et al. Nix is a selective autophagy receptor for mitochondrial clearance. *EMBO Rep.* 2010;11(1):45-51.

13. Sandoval H, Thiagarajan P, Dasgupta SK, et al. Essential role for Nix in autophagic maturation of erythroid cells. *Nature*. 2008;454(7201):232-235.
14. Schweers RL, Zhang J, Randall MS, et al. NIX is required for programmed mitochondrial clearance during reticulocyte maturation. *Proc Natl Acad Sci U S A*. 2007;104(49):19500-19505.
15. Matsuda N, Sato S, Shiba K, et al. PINK1 stabilized by mitochondrial depolarization recruits Parkin to damaged mitochondria and activates latent Parkin for mitophagy. *J Cell Biol*. 2010;189(2):211-221.
16. Ordureau A, Paulo JA, Zhang W, et al. Dynamics of PARKIN-Dependent Mitochondrial Ubiquitylation in Induced Neurons and Model Systems Revealed by Digital Snapshot Proteomics. *Mol Cell*. 2018;70(2):211-227.
17. Narendra DP, Jin SM, Tanaka A, et al. PINK1 is selectively stabilized on impaired mitochondria to activate Parkin. *PLoS Biol*. 2010;8(1):e1000298.
18. Sun Y, Vashisht AA, Tchieu J, Wohlschlegel JA, Dreier L. Voltage-dependent anion channels (VDACs) recruit Parkin to defective mitochondria to promote mitochondrial autophagy. *J Biol Chem*. 2012;287(48):40652-40660.
19. Geisler S, Holmstrom KM, Skujat D, et al. PINK1/Parkin-mediated mitophagy is dependent on VDAC1 and p62/SQSTM1. *Nat Cell Biol*. 2010;12(2):119-131.
20. Gatliff J, East D, Crosby J, et al. TSPO interacts with VDAC1 and triggers a ROS-mediated inhibition of mitochondrial quality control. *Autophagy*. 2014;10(12):2279-2296.
21. Shoshan-Barmatz V, Keinan N, Abu-Hamad S, Tyomkin D, Aram L. Apoptosis is regulated by the VDAC1 N-terminal region and by VDAC oligomerization: release of cytochrome c, AIF and Smac/Diablo. *Biochim Biophys Acta*. 2010;1797(6-7):1281-1291.
22. Shimizu S, Narita M, Tsujimoto Y. Bcl-2 family proteins regulate the release of apoptogenic cytochrome c by the mitochondrial channel VDAC. *Nature*. 1999;399(6735):483-487.
23. Rone MB, Midzak AS, Issop L, et al. Identification of a dynamic mitochondrial protein complex driving cholesterol import, trafficking, and metabolism to steroid hormones. *Mol Endocrinol*. 2012;26(11):1868-1882.
24. Lee AC, Xu X, Colombini M. The role of pyridine dinucleotides in regulating the permeability of the mitochondrial outer membrane. *J Biol Chem*. 1996;271(43):26724-26731.
25. Rostovtseva TK, Komarov A, Bezrukov SM, Colombini M. VDAC channels differentiate between natural metabolites and synthetic molecules. *J Membr Biol*. 2002;187(2):147-156.
26. An X, Schulz VP, Li J, et al. Global transcriptome analyses of human and murine terminal erythroid differentiation. *Blood*. 2014;123(22):3466-3477.

27. Gautier EF, Ducamp S, Leduc M, Salnot V, Guillonneau F, Dussiot M, et al. Comprehensive Proteomic Analysis of Human Erythropoiesis. *Cell Rep.* 2016;16(5):1470-1484.
28. Hu J, Liu J, Xue F, et al. Isolation and functional characterization of human erythroblasts at distinct stages: implications for understanding of normal and disordered erythropoiesis in vivo. *Blood.* 2013;121(16):3246-3253.
29. Konstantinidis DG, Pushkaran S, Johnson JF, et al. Signaling and cytoskeletal requirements in erythroblast enucleation. *Blood.* 2012;119(25):6118-6127.
30. Wang J, Ramirez T, Ji P, Jayapal SR, Lodish HF, Murata-Hori M. Mammalian erythroblast enucleation requires PI3K-dependent cell polarization. *J Cell Sci.* 2012;125(Pt 2):340-349.
31. Gasko O, Danon D. Deterioration and disappearance of mitochondria during reticulocyte maturation. *Exp Cell Res.* 1972;75(1):159-169.
32. Simpson CF, Kling JM. The mechanism of mitochondrial extrusion from phenylhydrazine-induced reticulocytes in the circulating blood. *J Cell Biol.* 1968;36(1):103-109.
33. Beams HW, Kessel RG. Electron microscope and ultracentrifugation studies on the rat reticulocyte. *Am J Anat.* 1966;118(2):471-507.
34. Bantug GR, Fischer M, Grahlert J, et al. Mitochondria-Endoplasmic Reticulum Contact Sites Function as Immunometabolic Hubs that Orchestrate the Rapid Recall Response of Memory CD8⁺ T Cells. *Immunity.* 2018;48(3):542-555.e6.
35. Pankiv S, Clausen TH, Lamark T, et al. p62/SQSTM1 binds directly to Atg8/LC3 to facilitate degradation of ubiquitinated protein aggregates by autophagy. *J Biol Chem.* 2007;282(33):24131-24145.
36. Vo MT, Smith BJ, Nicholas J, Choi YB. Activation of NIX-mediated mitophagy by an interferon regulatory factor homologue of human herpesvirus. *Nat Commun.* 2019;10(1):3203.
37. Liu X, Zhang Y, Ni M, et al. Regulation of mitochondrial biogenesis in erythropoiesis by mTORC1-mediated protein translation. *Nat Cell Biol.* 2017;19(6):626-638.
38. Moras M, Hattab C, Gonzalez-Menendez P, et al. Downregulation of Mitochondrial TSPO Inhibits Mitophagy and Reduces Enucleation during Human Terminal Erythropoiesis. *Int J Mol Sci.* 2020;21(23).
39. Yang C, Hashimoto M, Lin QXX, Tan DQ, Suda T. Sphingosine-1-phosphate signaling modulates terminal erythroid differentiation through the regulation of mitophagy. *Exp Hematol.* 2019;72:47-59.
40. Gilquin B, Taillebourg E, Cherradi N, et al. The AAA+ ATPase ATAD3A controls mitochondrial dynamics at the interface of the inner and outer membranes. *Mol Cell Biol.* 2010;30(8):1984-1996.

41. Jin G, Xu C, Zhang X, et al. Atad3a suppresses Pink1-dependent mitophagy to maintain homeostasis of hematopoietic progenitor cells. *Nat Immunol.* 2018;19(1):29-40.
42. Greene AW, Grenier K, Aguilera MA, et al. Mitochondrial processing peptidase regulates PINK1 processing, import and Parkin recruitment. *EMBO Rep.* 2012;13(4):378-385.
43. Heo JM, Harper NJ, Paulo JA, et al. Integrated proteogenetic analysis reveals the landscape of a mitochondrial-autophagosome synapse during PARK2-dependent mitophagy. *Sci Adv.* 2019;5(11):eaay4624.
44. Hoshino A, Wang WJ, Wada S, et al. The ADP/ATP translocase drives mitophagy independent of nucleotide exchange. *Nature.* 2019;575(7782):375-379.
45. Traxler EA, Thom CS, Yao Y, Paralkar V, Weiss MJ. Nonspecific inhibition of erythropoiesis by short hairpin RNAs. *Blood.* 2018;131(24):2733-2736.
46. Lupo F, Tibaldi E, Matte A, et al. A new molecular link between defective autophagy and erythroid abnormalities in chorea-acanthocytosis. *Blood.* 2016;128(25):2976-2987.
47. Jagadeeswaran R, Vazquez BA, Thirupathi M, et al. Pharmacological inhibition of LSD1 and mTOR reduces mitochondrial retention and associated ROS levels in the red blood cells of sickle cell disease. *Exp Hematol.* 2017;50:46-52.
48. Jiang H, Yang L, Guo L, et al. Impaired Mitophagy of Nucleated Erythroid Cells Leads to Anemia in Patients with Myelodysplastic Syndromes. *Oxid Med Cell Longev.* 2018;2018:6328051.
49. Sbardella D, Tundo GR, Campagnolo L, et al. Retention of Mitochondria in Mature Human Red Blood Cells as the Result of Autophagy Impairment in Rett Syndrome. *Sci Rep.* 2017;7(1):12297.
50. Wu L, Xu W, Xu L, Kong Q, Fang J. Mitophagy is increased during erythroid differentiation in beta-thalassemia. *Int J Hematol.* 2017;105(2):162-173.
51. Li-Harms X, Milasta S, Lynch J, et al. Mito-protective autophagy is impaired in erythroid cells of aged mtDNA-mutator mice. *Blood.* 2015;125(1):162-174.
52. Houwerzijl EJ, Pol HW, Blom NR, van der Want JJ, de Wolf JT, Vellenga E. Erythroid precursors from patients with low-risk myelodysplasia demonstrate ultrastructural features of enhanced autophagy of mitochondria. *Leukemia.* 2009;23(5):886-891.
53. Koschade SE, Brandts CH. Selective Autophagy in Normal and Malignant Hematopoiesis. *J Mol Biol.* 2020;432(1):261-282.

Figure Legends

Figure 1. VDAC1 knockdown in human erythroid progenitors accelerates erythroid differentiation. (A) Schematic of the *ex vivo* erythroid differentiation protocol following shRNA-mediated downregulation of VDAC1 (CBMC, Cord Blood Mononucleated Cells; shSCR, Scramble shRNA; shVDAC1, VDAC1 shRNA). CD34⁺ progenitors were isolated from cord blood and transduced at day 4 with a lentiviral vector harboring either the VDAC1 shRNA or Scramble shRNA, together with the EGFP transgene. EGFP⁺ cells were sorted at day 7 and differentiated until day 17. (B) Representative MGG images of erythroid progenitors and quantification of cells at different stages of differentiation are shown for day 7 and (C) day 10 of differentiation (n = 3). Scale bar = 20 μ m. (D) Representative α 4-integrin/Band3 flow cytometry profiles of GPA⁺ cells at day 10 are shown, allowing different stages of differentiation to be distinguished. (E) Band3 and (F) α 4-integrin surface expressions were evaluated on GPA⁺ cells following introduction of shSCR (black) and shVDAC1 (red) at days 8, 10, 14, and 16 of erythroid differentiation. The percentages at each time point were quantified and means \pm S.E. are shown (n = 9). (G) Erythroblast proliferation in control progenitors and shVDAC1-transduced progenitors was monitored at days 7, 10, 14 and 17 (n = 4). *p<0.05, **p<0.01, *** p<0.001.

Figure 2. Enucleation is impaired in shVDAC1-transduced erythroid progenitors. (A) The progression of terminal erythroid progenitors to the reticulocyte stage of differentiation was evaluated following shSCR and shVDAC1 transduction. Representative MGG images (left) and quantification of the different progenitor stages (right) at day 14 and (A) day 17 (B) are presented and means \pm S.E. are shown. Scale bar = 20 μ m. (C) The percentages of enucleated cells (GPA⁺, Hoechst⁻ cells) were quantified by flow cytometry at day 10, 14 and 17 of differentiation (n = 4) and means \pm S.E. are shown. (D) Apoptosis was evaluated by Annexin V staining and the quantification of Annexin V⁺ cells is presented at day 7, 10, 14 and 17 (n = 3). *p<0.05, **p<0.01, ****p<0.0001.

Figure 3. VDAC1 downregulation causes a retention of mitochondria in late stage erythroblasts. (A) Mitochondrial mass was measured by Mitofluor staining in erythroblasts at different stages of terminal differentiation and representative histograms (left) and quantification of the mean fluorescence intensity (MFI) are shown (n = 5) (right). (B) Levels of the mitochondrial protein TOM40 were quantified by immunoblot at day 10 of differentiation and representative blots (left) as well as normalization to β -actin (right) are presented. Levels in control cells was arbitrarily set at “1” (n = 5). (C) Mitochondrial content of erythroblasts at day 11 of differentiation was evaluated by Mitofluor staining on basophilic, polychromatic and orthochromatic erythroblasts and MFI in progenitors transduced with shSCR (black dots) and shVDAC1 (red dots) transduced cells are presented (n = 5). Gates for erythroblasts populations are based on α 4-integrin/Band3 profiles as shown in Figure 1D. *p<0.05, **p<0.01.

Figure 4. Mitochondria morphology is altered and oxidative phosphorylation is attenuated upon VDAC1 downregulation. (A) Sample TEM images of erythroblasts at day 10 of differentiation (black arrows show ER-mitochondria contact site) with swollen cristae indicated by red arrows. Scale bar = 200 nm. (B) TEM-based quantification of the percentage of altered cristae and (C) number of rounded (white) and elongated (black) mitochondria by μ m² are presented. (D) The number of mitochondria-ER contact site by μ m² is presented.

Quantification in 20 for panels B and C and 9 different cells for panel D. * $p < 0.05$, *** $p < 0.001$, **** $p < 0.0001$. (E) Oxygen consumption rates (OCR) were monitored in the indicated populations at day 10 of differentiation by Seahorse technology and representative profiles are formed ($n > 3$ technical replicates). Data were normalized to mitochondrial quantity using MFI values of Mitotracker Deep Red previously measured by flow cytometry. (F) Basal and maximum respiration were quantified with levels in control cells arbitrarily set at “1” ($n = 3$). (G) Intracellular ATP in shSCR- and shVDAC1-transduced erythroblasts was evaluated at day 10 of differentiation by luminometry with levels in control cells arbitrarily set at “1” ($n = 3$). Data are presented as means \pm S.E. * $p < 0.05$, *** $p < 0.001$.

Figure 5. Autophagy is impaired in VDAC1 shRNA-transduced cells. (A) Schematic representation of the role of the PINK1/Parkin and NIX pathways in mitochondrial degradation. (B) LC3-I and LC3-II levels were evaluated in shSCR- and shVDAC1-transduced erythroblasts at day 10 and representative immunoblots are presented (left). LC3-II levels were normalized to β -actin with levels in control cells arbitrarily set at “1” ($n = 5$) (right). (C) p62 levels were monitored and representative immunoblots (left) and quantifications (right) are presented. p62 levels were normalized to β -actin with levels in control cells arbitrarily set at “1” ($n = 6$). (D) p62 protein level was evaluated by flow cytometry on basophilic, polychromatic ($n = 8$) and orthochromatic erythroblasts ($n = 3$) and MFI of shSCR (black dots) and shVDAC1 (red dots) are presented with levels in control cells arbitrarily set at “1”. Gates for erythroblasts populations are based on $\alpha 4$ -integrin/Band3 profiles as shown in Figure 1D. * $p < 0.05$. (E) Colocalization of LC3 and TOM22 was monitored by confocal microscopy and representative images are shown. Scale bar = 3 μ m. (left) The Pearson coefficient between LC3 and TOM22 are presented for 30 cells in a representative experiment ($n = 3$) (right). n.s., non-significant, * $p < 0.05$, ** $p < 0.01$, **** $p < 0.0001$.

Figure 6. Lower PINK1 protein levels upon VDAC1 downregulation. (A) PINK1 levels were evaluated by immunoblot in the indicated conditions at day 10 of differentiation and normalized to the quantity of mitochondria (housekeeping mitochondrial TOM40) on total number of cell (housekeeping β -actin) (top). Levels in control cells were arbitrarily set at “1” ($n = 5$) (bottom). (B) PINK1 protein level was evaluated by flow cytometry on basophilic, polychromatic ($n = 8$) and orthochromatic erythroblasts ($n = 3$). PINK1 MFI was normalized to mitochondrial housekeeping TOM22 MFI in erythroblasts transduced with shSCR (black dots) and shVDAC1 (red dots), with levels in control cells arbitrarily set at “1”. Gates for erythroblasts populations are based on $\alpha 4$ -integrin/Band3 profiles as shown in Figure 1D. (C) PINK1 protein levels were evaluated by immunoblot in the indicated conditions in shSCR-K562 and shVDAC1-K562 cells and normalized to the quantity of mitochondria marker TOM40 on total number of cell (β -actin). Levels in control cells were arbitrarily set at “1” ($n = 4$). (D) PINK1/TOM22 colocalization (MPI ratio from PINK1 and TOM22 signals) assessed by imaging flow cytometry of shSCR-K562 and shVDAC1-K562 cells ($n = 3$). (E) LC3/TOM22 colocalization assessed by imaging flow cytometry (MPI ratio from LC3 and TOM22 signals) of shSCR-K562 and shVDAC1-K562 cells and shSCR-K562 cells transfected with a PINK1 siRNA ($n = 3$). n.s., non-significant, * $p < 0.05$, *** $p < 0.001$, **** $p < 0.0001$.

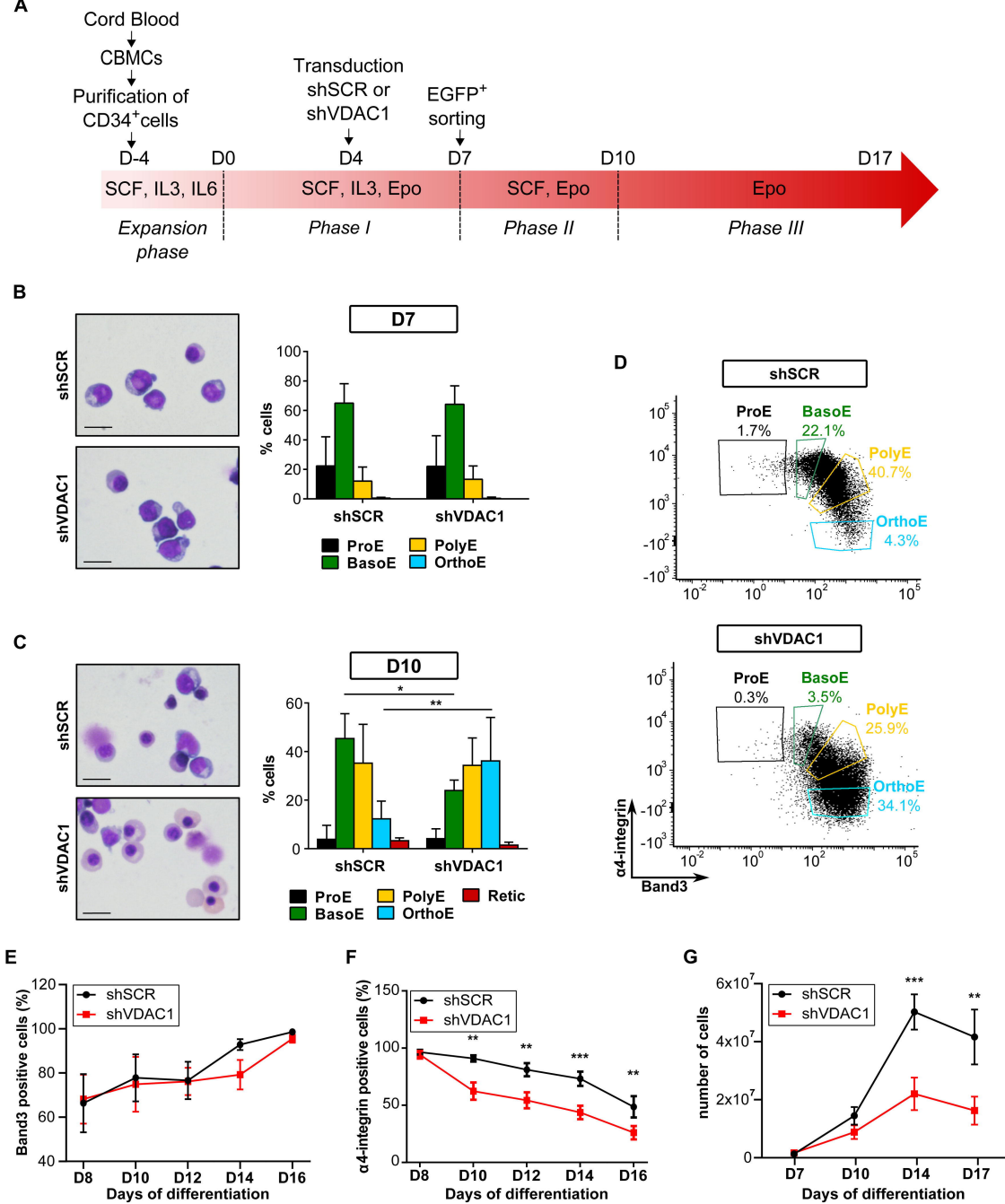


Figure 1. Moras et al.

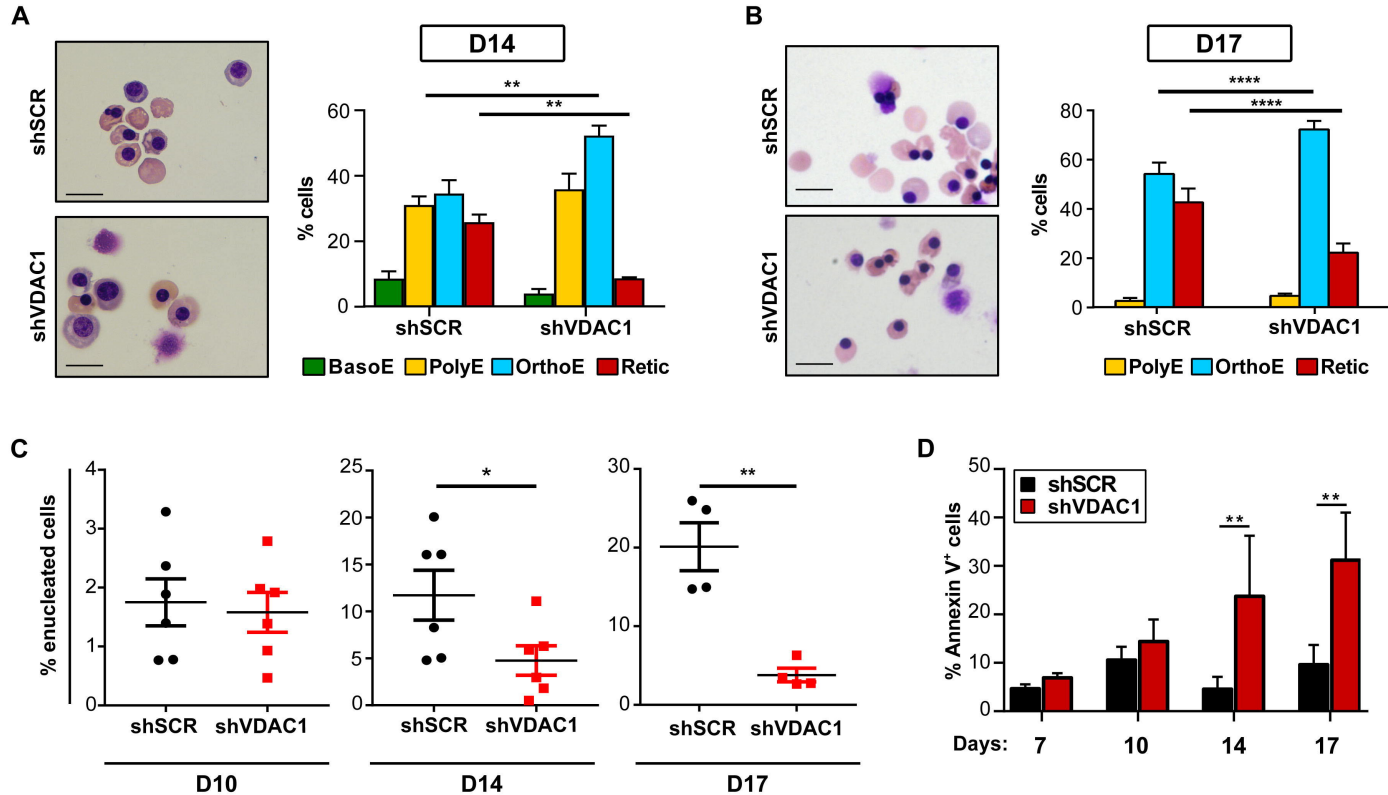


Figure 2. Moras et al.

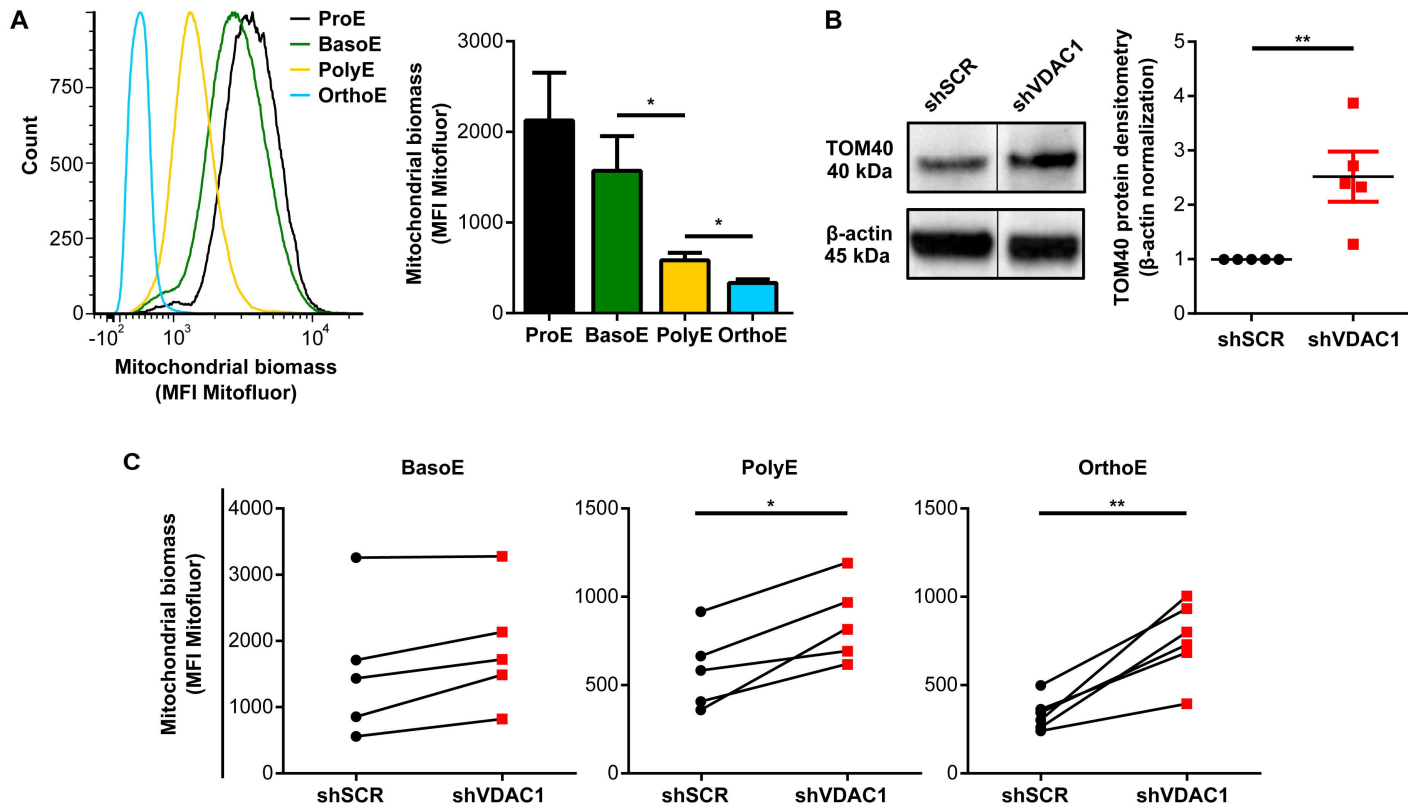


Figure 3. Moras et al.

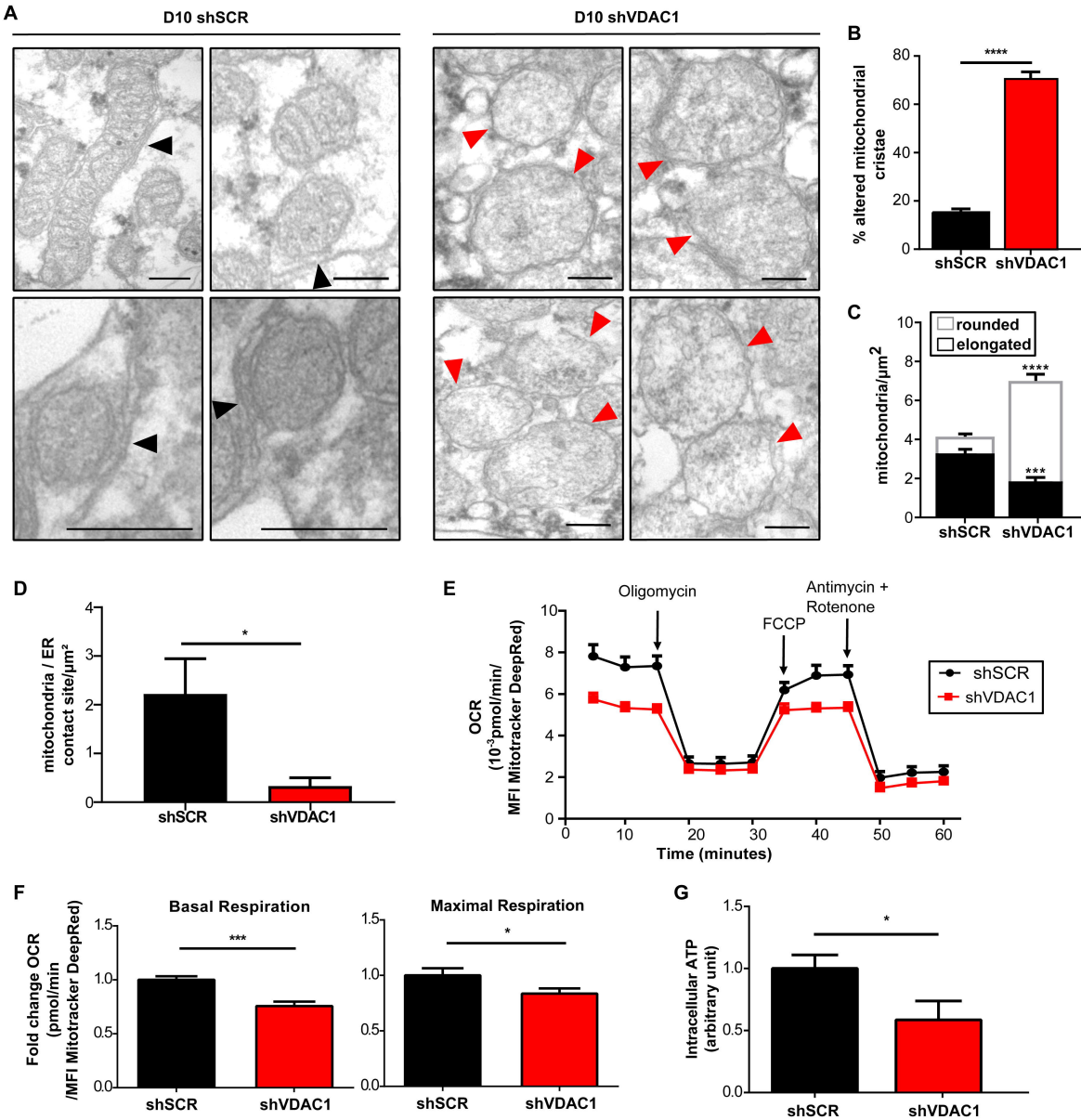


Figure 4. Moras et al.

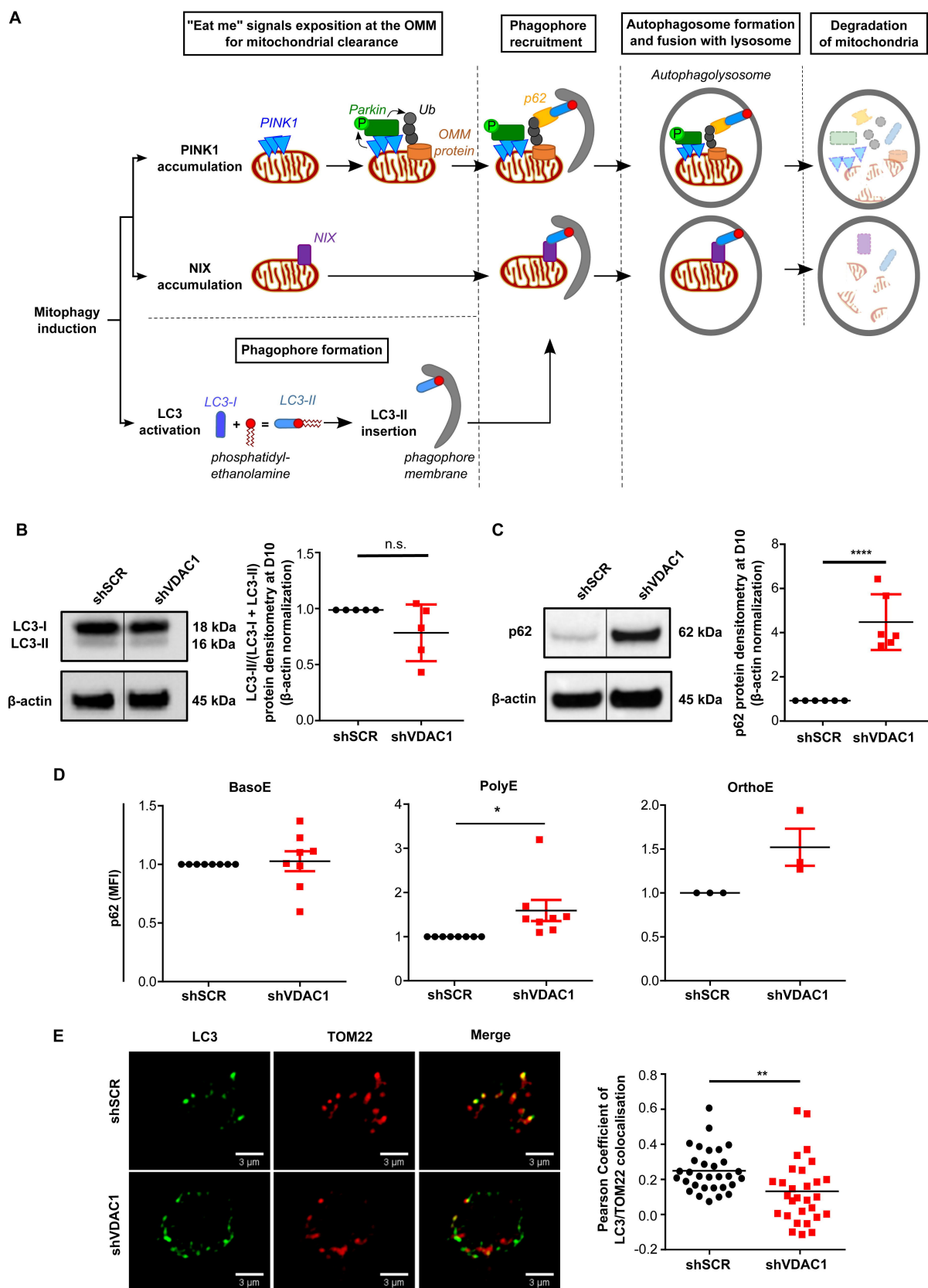


Figure 5. Moras et al.

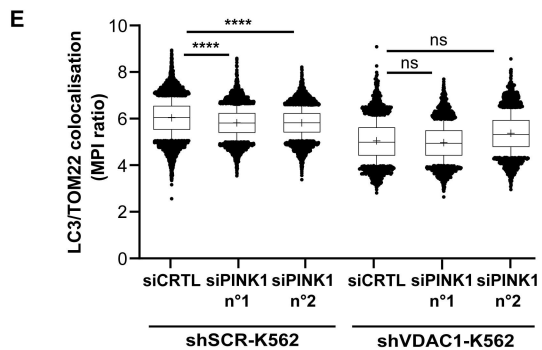
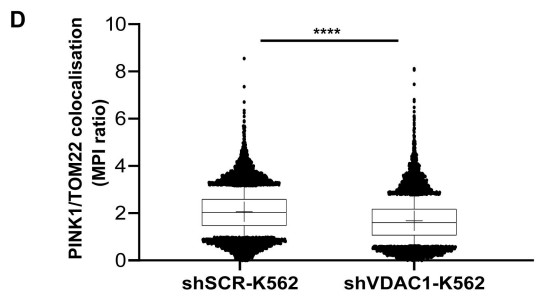
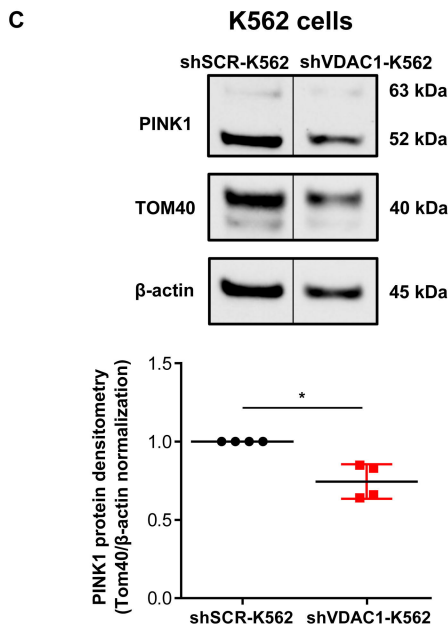
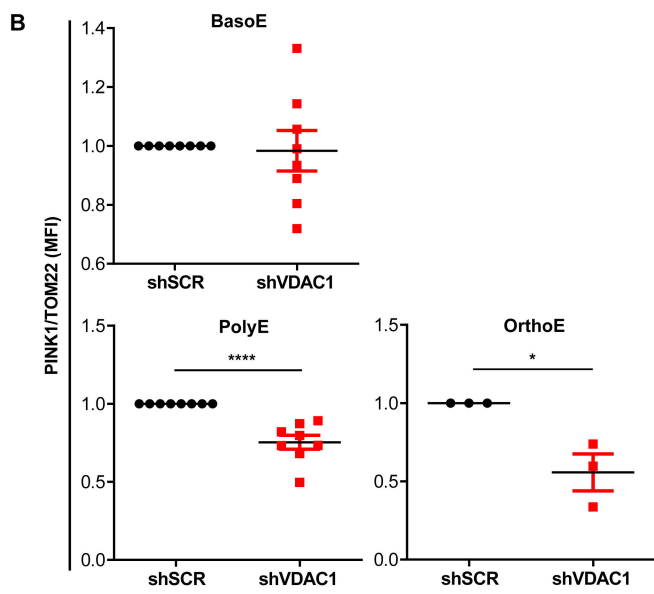
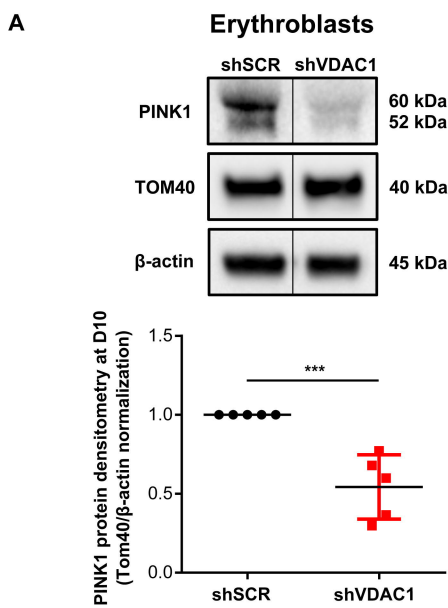


Figure 6. Moras et al.

Human erythroid differentiation requires VDAC1-mediated mitochondrial clearance

Martina Moras^{1,2,3}, Claude Hattab^{1,2,3}, Pedro Gonzalez-Menendez^{3,4}, Claudio M. Fader^{5,6}, Michael Dussiot⁷, Jerome Larghero⁸, Caroline Le Van Kim^{1,2,3}, Sandrina Kinet^{3,4}, Naomi Taylor^{3,4,9}, Sophie D. Lefevre^{1,2,3*#}, Mariano A. Ostuni^{1,2,3*#}

Running Head: **VDAC-driven mitophagy in human erythropoiesis**

corresponding authors

Mariano A. OSTUNI and Sophie D. LEFEVRE

UMR_S1134 Biologie Intégrée du Globule Rouge

6, rue Alexandre Cabanel

75739 Paris cedex 15, FRANCE

Email address: mariano.ostuni@inserm.fr; sophie.lefevre@inserm.fr

Phone: +33 1 44 49 31 35

Fax: +33 1 43 06 50 19

Supplementary Methods

Purification and culture of CD34⁺ cells

Cord blood mononuclear cells (CBMCs) from healthy donors were used in this study. Umbilical cord blood that cannot be qualified for the use in patients was obtained from the center for biological resources from Saint-Louis Hospital Cord Blood Bank registered to the French Ministry of Research under number AC-2016-2756, and to the French Normalization Agency under number 201/51848.1. This study was approved and conducted according to institutional ethical guidelines of the National Institute for Blood Transfusion (N°2019-1, INTS, Paris, France). It was also approved by the Ethics committee of INSPIRE program (Horizon 2020 grant agreement 665850). All procedures were carried out in accordance to the Declaration of Helsinki. Written informed consent was given by the donors. PBMCs were separated from whole blood using Ficoll (GE healthcare) and CD34⁺ cells were purified from cord blood by positive selection using the magnetic-activated cell sorting magnetic beads system (Miltenyi Biotec), according to the manufacturer's instructions.

CD34⁺ cells were cultured in Iscove's Modified Dulbecco's Medium (Invitrogen), 2% human peripheral blood plasma (Stem Cell Technologies), 3% human AB serum (Sigma Aldrich), 15% BIT 9500 Serum Substitute (Stem Cell Technologies) and 3 IU/mL heparin (Sigma Aldrich). For the expansion phase (day -4 to day 0), cells were seeded at a concentration of 10⁵ cells/mL in culture medium supplemented with 25 ng/mL stem cell factor (SCF, Miltenyi Biotec), 10 ng/mL IL-

3 (Miltenyi Biotec) and 10 ng/mL IL-6 (Miltenyi Biotec). In the phase I (day 0 to day 6), medium was supplemented with 10 ng/mL SCF, 1 ng/mL IL-3 (Miltenyi Biotec) and 3 IU/mL erythropoietin. IL-6 was omitted from the culture medium. In the phase II (day 7 to day 10), IL-3 was omitted from the culture medium. In the phase III (that lasted until day 17) SCF was omitted.

VDAC1 silencing plasmid and lentiviral production

Lentiviruses particles were produced by co-transfection of HEK293T cells with the plasmids MISSION® pLKO.1-puro Non-Target shRNA Control Plasmid DNA or shVDAC1 (TRCN0000297481, responding sequence, 5'-GCAGTTGGCTACAAGACTGAT-3') with the 714bp EGFP sequence that was inserted in place of the puromycin gene at the unique BamHI and KpnI restriction sites, together with the helper plasmids Δ 8.9 and VSV-G in HBS buffer (454 μ M NaCl, 23 mM Na₂HPO₄, 28 mM KCl, 216 mM dextrose, pH = 7.05) and 132 mM CaCl₂. On the following day, the medium was replaced with DMEM without serum, and the cells were cultured for 1 day before the supernatant containing viruses was collected. Viruses were concentrated by OVN centrifugation at 4000 rpm at 4 °C.

Cell Culture and small interference (siRNA) or short hairpin (shRNA) transfection

K562 cells were maintained in RPMI 1640 medium (ThermoFischer, France), supplemented with 10 % fetal calf serum and 1 % antibiotics penicillin-streptomycin. The cells were incubated at 37°C in a humidified atmosphere with 5 % CO₂ and 95 % air. K562 cells in exponential phase were transfected by electroporation (Amaxa, Nucleofector Kit V, France) with MISSION® pLKO.1-puro plasmids. shSCR-K562 and shVDAC1-K562 stable cell lines were created using puromycin selection. For mitophagy induction, cells were challenged with 50 μ M CCCP for 4 hours at 37°C. Cells were then transfected with one of the following small-interfering (si)RNA duplexes (ThermoFisher scientific, France): Ambion® Silencer® Negative Control #5 siRNA (AM4642), VDAC1 siRNA (s14769), PINK1 siRNA n°1 (s35166) and PINK1 siRNA n°2 (s35168).

Antibodies and dyes

The following antibodies (Ab) and corresponding dilution were used for Western blotting: monoclonal mouse anti-VDAC1 Ab (Santa Cruz, sc-390996, 1:500), rabbit anti-MAP LC3B Ab (Sigma Aldrich, L7543, 1:200), rabbit anti-p62 Ab (GeneTex, GTX100685, 1:1,000), rabbit anti-PINK1 (GeneTex, GTX107851, 1:1000),), rabbit anti-BNIP3L (GeneTex, GTX111876, 1:1000), mouse anti-TOM40 Ab (Santa Cruz, sc-365467, 1:1000), HRP-coupled anti-rabbit Ab (Jackson, 111-035-144, 1:5000), HRP-coupled anti-mouse (Jackson, 115-035-003, 1:5000), HRP-coupled anti-actin Ab (Cell signaling, 13E5, 1:3,000). For immunostaining: mouse anti-TOM22 (Abcam,

ab57523, 20 µg/mL), rabbit anti-MAP LC3B Ab (Sigma Aldrich, L7543, 1:100), Alexa Fluor 568 Goat anti-rabbit IgG Ab and Alexa Fluor 633 Goat anti-mouse IgG Ab (Thermo Fisher Scientific, 1:200). PE-conjugated mouse anti-human Band3 (IBGRL, 9439PE BRIC 6, 1:50), PE-Cy7-conjugated mouse anti-human CD235a (BD Pharmingen™, 563666, 1:20), APC-H7-conjugated mouse anti-human CD49d (BD Pharmingen™, 656153, 1:10) were used for flow cytometry. Mitotracker (MitoFluor Red 589 (M-22424), 250 nM or Mitotracker Deep Red (M22426), 50 nM) were used for mitochondria staining. Hoechst 34580 (BD Pharmingen™, 1 µg/mL) was used for enucleation assay in imaging flow cytometry and Hoechst 33342 (BD Pharmingen™, 1 µg/mL) was used for flow cytometry-based analysis of erythroid differentiation. PE-coupled Annexin V (BD Pharmingen™, 1:20) were used for viability assay in flow cytometry. 7-Aminoactinomycin D (7AAD, Thermo Fisher Scientific, 1:200) was used as viability staining in flow cytometry.

MGG-based identification of erythroblasts stage

10^5 of total and sorted cells according to $\alpha 4$ -integrin and Band3 surface expression as described by Hu et al. 2013 (1), were cytopun using the Thermo Scientific Shandon 4 Cytospin to validate the gates. The slides were stained with May-Grunwald (Sigma Aldrich, MG500) solution for 5 min, with May-Grunwald solution diluted by half for other 5 min, and subsequently stained with Giemsa solution (Sigma Aldrich, GS500) diluted 10 times for 15 min. Cells were imaged using a Nikon Eclipse Ti-S inverted microscope with a 40x/0.6 Plan Fluor objective.

Apoptosis assay

Cells were washed in PBS and then resuspended in 100 µL of Annexin Buffer containing PE-coupled Annexin V. After 15 min of incubation at room temperature in the dark, 400 µL of Annexin buffer was added. Viability was assessed by flow cytometry.

Seahorse analysis

Oxygen consumption rate (OCR) was measured using the Seahorse XFe-96 Extracellular Flux Analyzer (Agilent). The day before the analysis the plate was calibrated with 200 µL of OVN calibration buffer per well at 37 °C. The following day the plate was coated with 100 µg/mL poly-D-lysine for 1h at RT. 3×10^5 cells were added in each well in XF media (non-buffered DMEM containing 10 mM glucose and 2 mM L-glutamine) and incubated at 37 °C without CO₂. The Mito Stress test was performed using 1 µM oligomycin, 1 µM FCCP, 100 nM rotenone and 1 µM antimycin A. After each addition inhibitor at least 3 sequential measurements were taken. Analysis of OCR data were performed using Wave software. As OCR values depend on the mitochondrial number, data were normalized using MFI values of Mitotracker Deep Red previously measured by flow cytometry.

SDS-PAGE and Immunoblotting

Whole-cell lysates of cultured cells were prepared buffer 10 mM Tris-HCl pH 6.8, 1 mM EDTA, 10% SDS, containing 1X cOmplete™ protease cocktail inhibitor (Roche). After sonication, cells were frozen for at least 1 h. Protein quantification was performed by Pierce™ BCA Protein Assay Kit (Thermo Fisher Scientific) and 30 µg of proteins were separated using NuPAGE® 4-12% Bis-Tris gels. After proteins transfer to a nitrocellulose membrane using Trans-Blot Turbo Transfer System (BioRad), immunoblotting was done with primary antibody overnight at 4 °C. Proteins of interest were revealed using HRP-conjugated secondary antibodies and the Enhanced Chemiluminescence kit (Perkin Elmer). Images were acquired by ChemiDoc™ Imaging Systems (Bio-Rad) and bands intensity were quantified with Image Lab software (Bio-Rad).

Quantitative real time qPCR

Total RNA was extracted using RNeasy kit (Qiagen) and quantified by NanoDrop 2000c (Thermo Scientific™). Reverse transcription of 2 µg of total RNA was performed using Multiscribe™ Reverse Transcriptase (Applied Biosystems) and gene expression assays were performed using QuantiNova SYBR Green RT-PCR Kit or QuantiNova Probe RT-PCR Kit (Qiagen). Primers used for assays were obtained from Eurofins MWG Operon. VDAC1 Fw 5'-AGCTGACCTTCGATTCATCCTTC-3' Rv 5'-TAATGTGCTCCCGCTTGTTACC-3', VDAC2 Fw 5'-AGTCTTGCAGTGGCGTGG-3' Rv 5'-TGGTCTCCAAGGTCCCAGTA-3', VDAC3 Fw 5'-CAGATGAGTTTTGACACAGCCA-3' Rv 5'-TCCAAATTCAGTGCCATCGTTC-3', NIX Fw 5'-GCCGGCCTCAACAGTTC-3' Rv 5'-TGGCATTGCGGAAAAGA-3'. Relative quantification of fold change was performed comparing Ct values from individual samples by applying the Pfaffl Method (2). Results were normalized for each of the samples by the expression of the TATA box binding protein (Prime Time® qPCR Assay, Hs.PT.58.19838260; Integrated DNA Technology).

Immunolabelling for confocal microscopy and imaging flow cytometry

Cells were fixed in 3% PFA and quenched with 50 mM NH₄Cl. Cells were permeabilized used 1% saponine/BSA (v/v in PBS) before staining overnight at 4 °C with primary antibodies. Cells were next incubated with AF546/AF647/AF633-conjugated Alexa secondary antibodies at RT for 1h in the dark. For confocal microscopy, 3x10⁵ cells were cytopun using Thermo Scientific Shandon 4 Cytospin and mounted with DAPI Fluoromount-G® (SouthernBiotech) before imaging with LSM 700 Laser Scanning Microscope (Zeiss) with a 63x/1.4 Oil Plan Apochromat objective. Zen and Fiji software were used to acquire images and process them, respectively. Colocalization tool from Imaris software (Oxford Instruments) was use for analyzing. After washing, 1 million cells were resuspended

in a total volume of 50 μ L and image acquisition was performed. Samples were run on an Imagestream ISX mkII (Amnis Corp, Luminex, Seattle, WA) and a 60X magnification was used for all acquisitions. Data were acquired using the INSPIRE software (Amnis Corp) and analyzed using the IDEASTM software (Version 6.2 Amnis Corp). On average, 30,000-50,000 events were collected in all experiments. Single stain controls were run for each fluorochrome used and spectral compensation was performed. Cells were gated for single cell using the area and aspect ratio of the brightfield image, then gated for focused cells using the gradient RMS feature; GFP positive cells were selected. A TOM mask was created to study its colocalization with PINK and LC3. TOM, PINK and LC3 quantification was expressed as mean pixel intensity value (MPI), which is the intensity normalized to surface area of the mask for TOM compartment. Colocalization was performed on double positive population and was determined by the ratio of the MPI of PINK or LC3 to the MPI of TOM, or using the Bright Detail Similarity R3 feature (BDS), which is the log transformed Pearson's correlation coefficient of the localized bright spots with a radius of 3 pixels within TOM mask between TOM and PINK or TOM and LC3. The Modulation feature, which measures the intensity range of an image, normalized between 0 and 1, was determined for LC3 in the cytoplasm mask. Modulation formula is $\text{Max Pixel} - \text{Min Pixel} / \text{Max Pixel} + \text{Min Pixel}$. Each result is the pool of 3 experiments.

ATP measurement by luminometer

Intracellular ATP was measured by quantitative luminometry using firefly luciferase, which catalyzes the oxidation of luciferin in the presence of ATP to produce light. 3×10^5 cells were frozen and resuspended in 150 μ L of water. 5 μ L of this lysate were added to 45 μ L of a luminometry mix (RBC medium containing 0.01 μ M luciferase, 0.2 mM luciferin, and 0.1 mg/mL of Coenzyme A), directly in the assay chamber of a custom-built luminometer as previously described (3), to determine the light intensity. Calibration of the luminometric signal was performed at the end of each measurement with ATP serial dilution from 1 μ M to 16 μ M.

Electron microscopy

After fixation with 2.5% glutaraldehyde, 10^6 erythroblasts (day 10 of differentiation) were post-fixed with osmium tetroxide 2% in cacodylate, pH 7.4, progressively dehydrated in acetone, and embedded in low-viscosity epoxy resin. 60-nm-thin sections were cut, mounted on copper grids, and stained with uranyl acetate and lead citrate. Sections were examined with a Zeiss EM900 electron microscope and archived with a CDD camera Gatan Orius CS1000.

Mitochondrial Morphology

As previously described (4), mitochondrial morphology was calculated from the Aspect Ratio, which is the ratio between the major and minor axis of the object considered as an ellipse. The result obtained determines the organelle length. These parameters, independent of the magnification of the image, have a minimum value of 1 corresponding to a circular shape of the mitochondria. Statistical tests were performed to compare the obtained images according to the different treatments. Mitochondria-ER contact sites were quantified following previously described protocols (5,6) adapted from (7)

ROS detection

Cells were stained with CellROX Deep Red Reagent (Thermo Fisher Scientific, C10422, 5 μ M) for total ROS staining, 30 min at 37 °C. After washing, cells were subsequently analyzed by flow cytometry.

Mitochondrial membrane potential assay

Cells were stained with MitoTracker™ Red CMXRos (Thermo Fisher Scientific, M7512, 250 nM) 30 min at 37 °C. After washing, cells were subsequently analyzed by flow cytometry.

Statistical Analysis

Each experiment was repeated at least 3 times, with a satisfactory correlation between the results of individual experiments. Statistical analyses were performed using Prism 6 (Graph Pad Software). Data were evaluated using the unpaired t-test and all comparisons with a p value less than 0.05 ($p < 0.05$) were considered statistically significant. $p < 0.0001$, $p < 0.001$, $p < 0.01$, and $p < 0.05$ are indicated with four, three, two, or one star (s), respectively. The data are expressed as the mean \pm the standard error of the mean (SEM).

References

1. Hu J, Liu J, Xue F, Halverson G, Reid M, Guo A, et al. Isolation and functional characterization of human erythroblasts at distinct stages: implications for understanding of normal and disordered erythropoiesis *in vivo*. *Blood*. 2013; 121(16):3246-53.
2. Pfaffl MW. A new mathematical model for relative quantification in real-time RT-PCR. *Nucleic acids research*. 2001; 29(9):e45.
3. Pafundo DE, Chara O, Faillace MP, Krumschnabel G, Schwarzbaum PJ. Kinetics of ATP release and cell volume regulation of hyposmotically challenged goldfish hepatocytes. *American journal of physiology Regulatory, integrative and comparative physiology*. 2008; 294(1):R220-33.

4. Vander Heiden MG, Chandel NS, Li XX, Schumacker PT, Colombini M, Thompson CB. Outer mitochondrial membrane permeability can regulate coupled respiration and cell survival. *Proceedings of the National Academy of Sciences of the United States of America*. 2000; 97(9):4666-71.
5. Modi S, López-Doménech G, Halff EF, Covill-Cooke C, Ivankovic D, Melandri D, et al. Miro clusters regulate ER-mitochondria contact sites and link cristae organization to the mitochondrial transport machinery. *Nat Commun*. 2019; 10(1):4399
6. Issop L, Fan J, Lee S, Rone MB, Basu K, Mui J, et al. Mitochondria-associated membrane formation in hormone-stimulated Leydig cell steroidogenesis: role of ATAD3. *Endocrinology*. 2015; 156(1):334-45.
7. Crowther RA, Amos LA, Finch JT, De Rosier DJ, Klug A. Three dimensional reconstructions of spherical viruses by fourier synthesis from electron micrographs. *Nature*; 226(5244):421-5.

Supplementary Figures

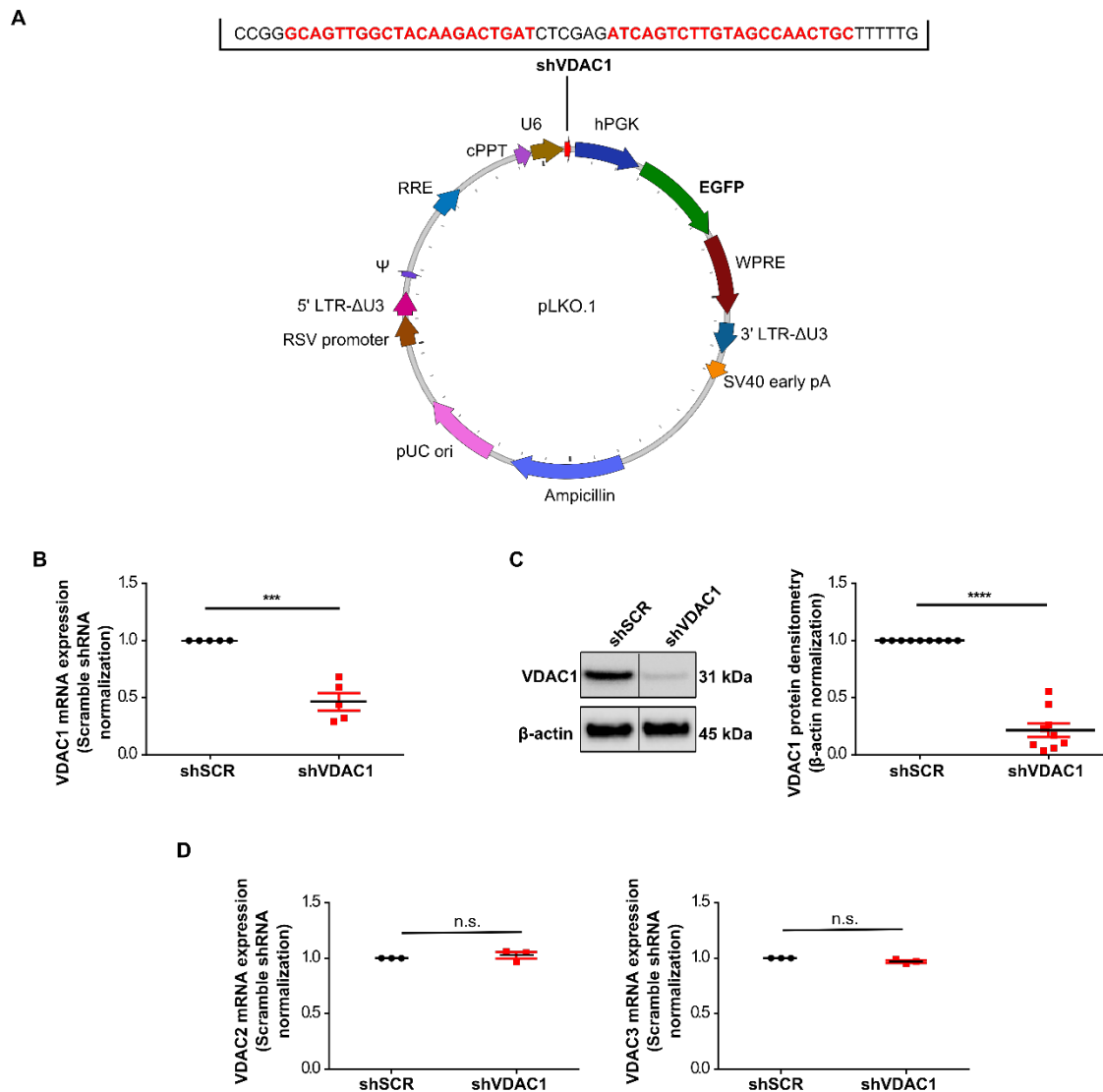


Figure S1. Downregulation of VDAC1 by a VDAC1-specific shRNA does not alter expression of VDAC2 or VDAC3 isoforms. (A) Map of the pLKO.1 vector showing the shVDAC1 insert sequence. (B) RT-qPCR (n = 5) and (C) Western Blot-based quantification (n = 9) of VDAC1 levels (day 10) (D) mRNA levels of VDAC2 and VDAC3 were evaluated in erythroblasts transduced with shSCR or shVDAC1 (n = 3). Levels in shSCR-transduced cells were arbitrarily set at “1”. Representative data and mean levels \pm S.E. are shown. *** $p < 0.001$, **** $p < 0.0001$.

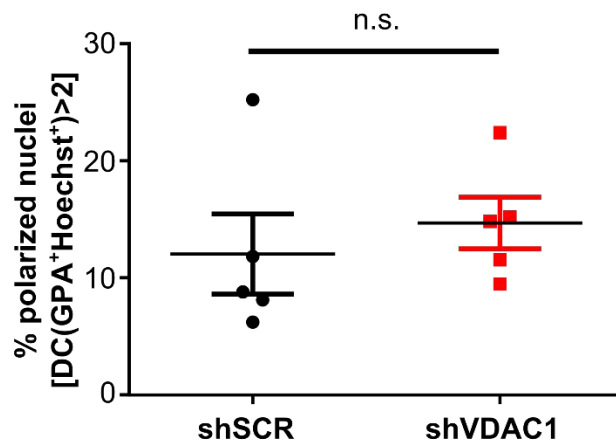
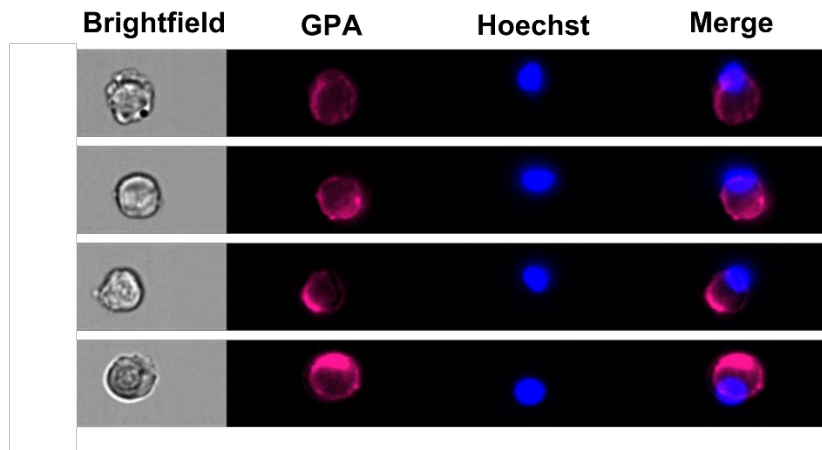


Figure S2. Downregulation of VDAC1 does not alter the polarization of the nuclei.

The presence of polarized nuclei was evaluated in FACS-purified orthochromatic erythroblasts 24 h post isolation by imaging flow cytometry. “Delta centroid GPA-Hoechst” (DC) with a threshold of 2 was arbitrary choose to discriminate polarized nuclei. Representative images (left) and quantification of polarized nuclei (right) in the different conditions are shown (n = 5).

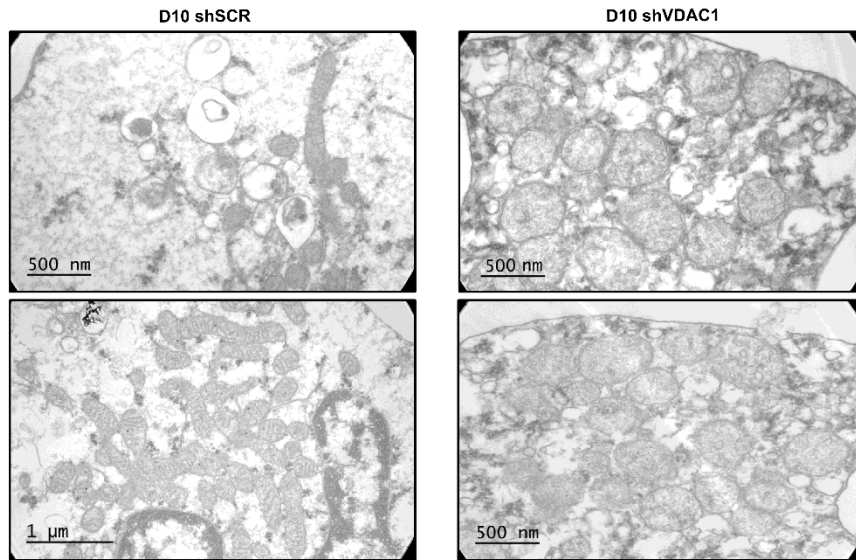


Figure S3. Mitochondria morphology is altered in erythroblasts following VDAC1 downregulation. Sample TEM images of erythroblasts at day 10 of differentiation.

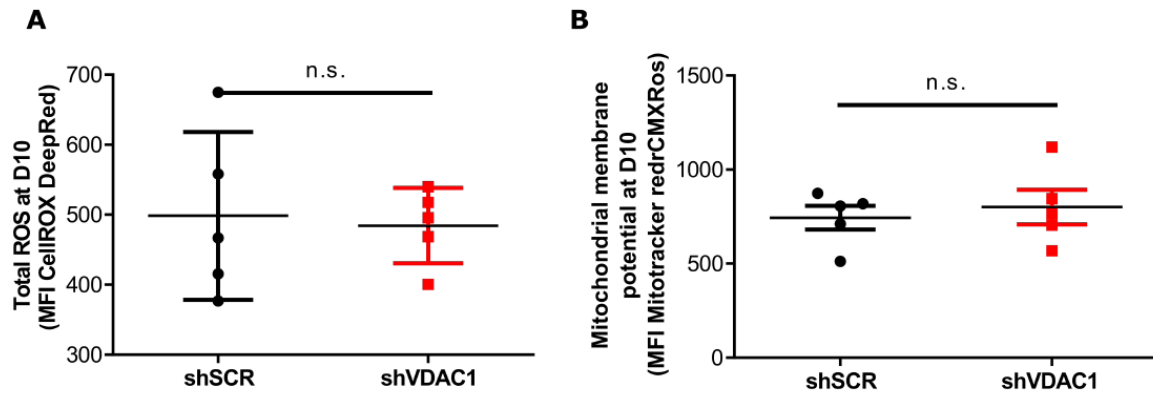


Figure S4. ROS production and mitochondrial membrane potential are not affected by downregulation of VDAC1. (A) Total ROS production quantification by flow cytometry (CellROX Deep Red Reagent) (n = 5) and (B) mitochondrial membrane potential (MitoTracker™ Red CMXRos) quantification measured at day 10 of differentiation (n = 5) and MFI of shSCR (black dots) and shVDAC1 (red dots) are presented.

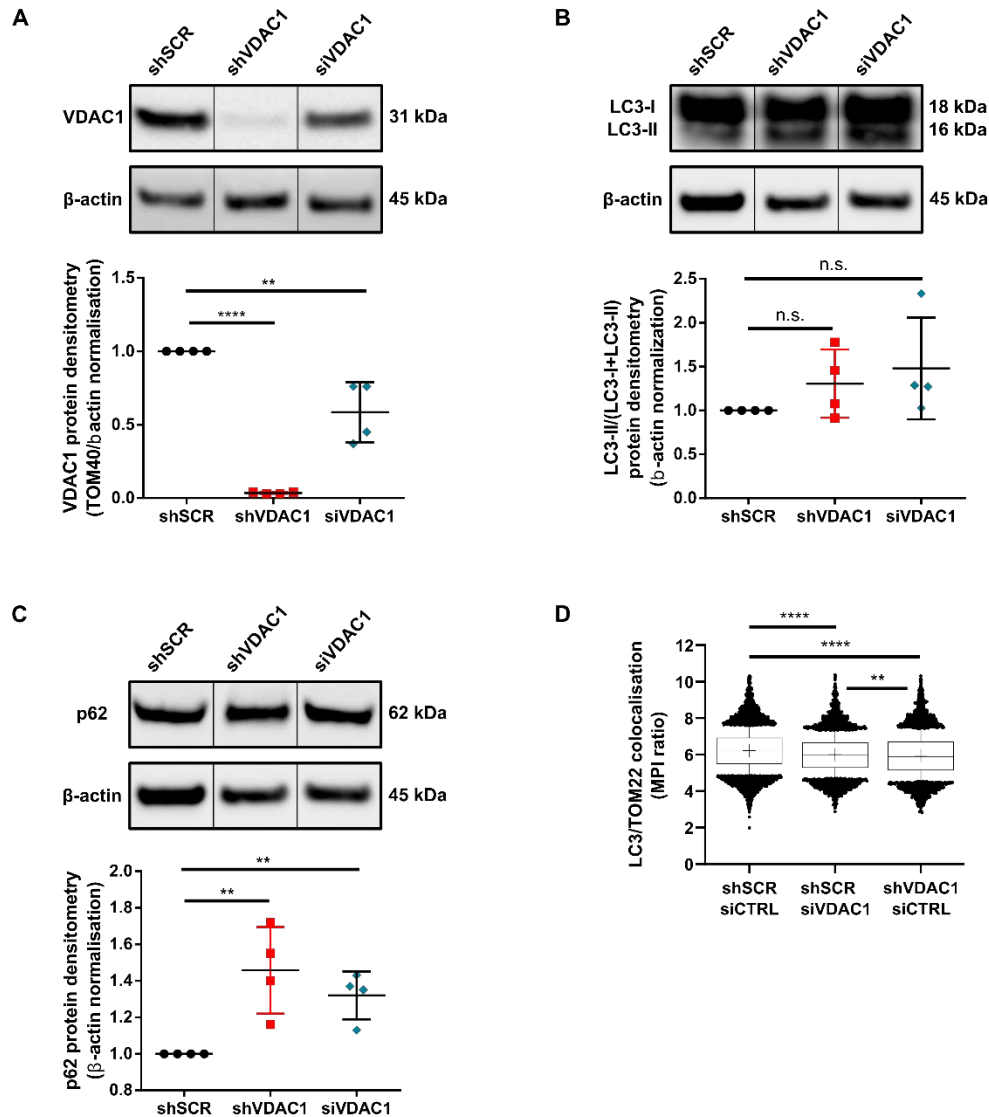


Figure S5. Lack of phagophore recruitment in shVDAC1-K562 cell line. (A) VDAC1 protein levels were evaluated by immunoblot in shSCR-K562, shVDAC1-K562 cell lines and VDAC1 siRNA-transfected shSCR-K562 cells and normalized to the quantity of mitochondria (TOM40) on total number of cell (β -actin). Levels in control cells were arbitrarily set at “1” ($n = 4$). (B) LC3-I and LC3-II levels were evaluated by immunoblots. LC3-II/total LC3 levels were normalized to β -actin with levels in control cells arbitrarily set at “1” ($n = 4$). (C) p62 levels were assessed by immunoblots and normalized to β -actin with levels in control cells arbitrarily set at “1” ($n = 4$). (D) LC3/TOM22 colocalization (MPI ratio) assessed by imaging flow cytometry of shSCR-K562 cells transfected or not with VDAC1 siRNA and shVDAC1-K562 cells ($n = 3$). ** $p < 0.01$, **** $p < 0.0001$

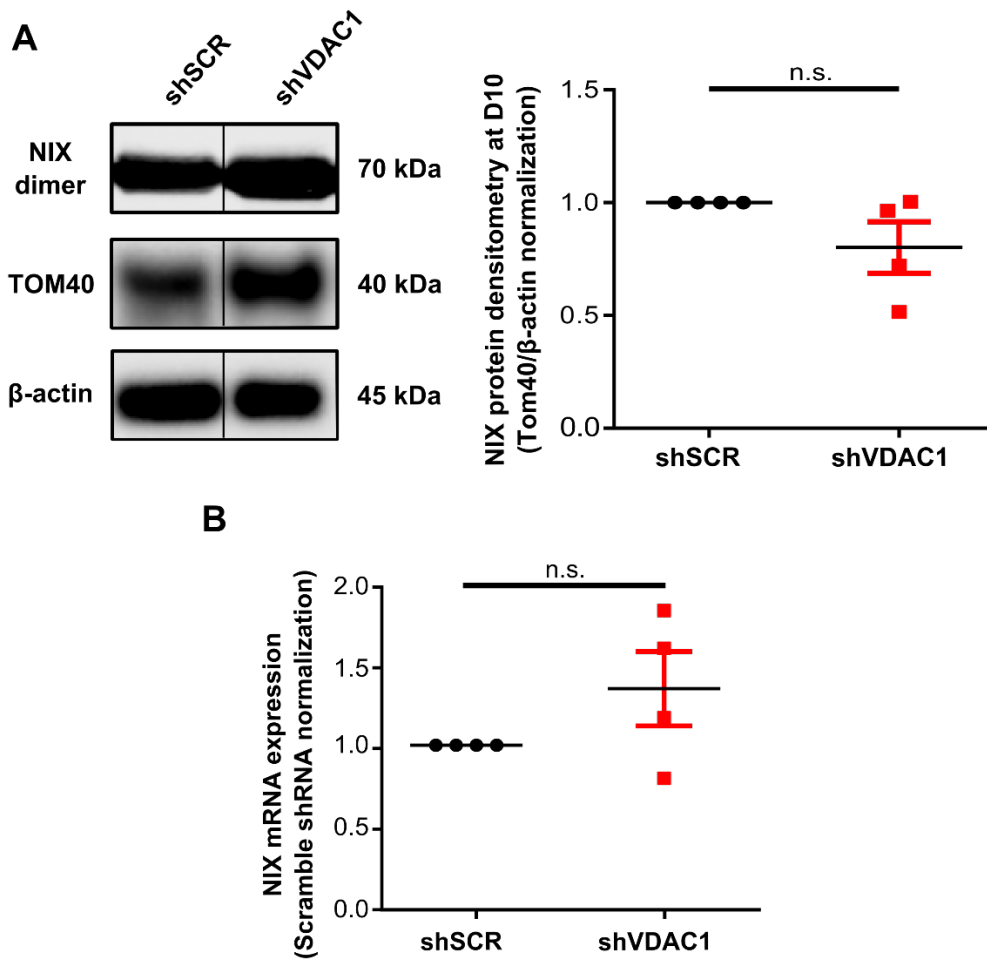


Figure S6. NIX levels are not affected by downregulation of VDAC1. (A) The presence of NIX dimers was assessed by Western Blot at day 10 of differentiation ($n = 4$) and normalized to the quantity of mitochondria (TOM40) on total number of cell (β -actin). (B) NIX mRNA levels were evaluated by RT-qPCR in sorted polychromatic cells and levels in shSCR-transduced cells were arbitrarily set at “1” ($n = 4$).